



**This electronic thesis or dissertation has been  
downloaded from Explore Bristol Research,  
<http://research-information.bristol.ac.uk>**

*Author:*  
**Withers, Emily G**

*Title:*  
**Resolution of the interaction site within 4R0N-tau mediating augmentation of L-type calcium current**

**General rights**

Access to the thesis is subject to the Creative Commons Attribution - NonCommercial-No Derivatives 4.0 International Public License. A copy of this may be found at <https://creativecommons.org/licenses/by-nc-nd/4.0/legalcode>. This license sets out your rights and the restrictions that apply to your access to the thesis so it is important you read this before proceeding.

**Take down policy**

Some pages of this thesis may have been removed for copyright restrictions prior to having it been deposited in Explore Bristol Research. However, if you have discovered material within the thesis that you consider to be unlawful e.g. breaches of copyright (either yours or that of a third party) or any other law, including but not limited to those relating to patent, trademark, confidentiality, data protection, obscenity, defamation, libel, then please contact [collections-metadata@bristol.ac.uk](mailto:collections-metadata@bristol.ac.uk) and include the following information in your message:

- Your contact details
- Bibliographic details for the item, including a URL
- An outline nature of the complaint

Your claim will be investigated and, where appropriate, the item in question will be removed from public view as soon as possible.

**UNIVERSITY OF BRISTOL**

**School of Physiology, Pharmacology and  
Neuroscience**

MSc by Research

Start date: October 2020

Deadline: October 2022

**Resolution of the interaction site within 4R0N-tau  
mediating augmentation of L-type calcium current**

**Author:** Emily Withers

Student No: 1609142

Email: emilywithers@live.com

**Supervisor:** Professor Neil Marrion

Email: N.V.Marrion@bristol.ac.uk

## **Acknowledgments**

I would like to thank my supervisor Neil Marrion for his amazing support and inspiration. I have developed so much passion for research from working with you.

I also want to thank Andrew Butler and Kevin Wilkinson for teaching me so many exciting techniques and being so willing to help. I don't think this thesis would exist without you!

Thank you to Dany Bozadzhieva, Ryan Cadman and James Charlick for making the lab a fun and supportive environment. Finally, thank you to the rest of my friends and family for helping motivate me throughout my masters and making my time in Bristol truly wonderful!

## **COVID-19 Impact Statement**

The COVID-19 pandemic was occurring throughout the entirety of my MRes. This presented some challenges to completing the project as our contact with supervisors was limited, meaning training on certain equipment took more time, and progress meetings were not happening as frequently as desired. This restricted the rate of progress of the MRes and the amount of work that could be done in the timeframe.

## Abstract

L-type calcium channels (LTCCs) are voltage gated calcium channels comprised of three subunits: an  $\alpha_1$  pore forming subunit and  $\beta$  and  $\alpha_2\delta$  auxillary subunits. LTCC's have a range of cellular functions, including activating potassium channels which are responsible for afterhyperpolarisations (AHPs): potentials which contribute to regulation of neuronal firing. Preliminary evidence suggests that 4R0N tau, a microtubule associated protein known to be overexpressed with age and in Alzheimer's disease (AD), can increase the amount of LTCC at the cell membrane of hippocampal neurons. This occurs if  $Ca_v1.2$  is the pore forming subunit for the LTCC and  $\beta_3$  is the  $\beta$  auxillary subunit. An increase in LTCCs at the cell membrane augments macroscopic calcium current and, subsequently, decreases the rate of neuronal firing by increasing the size of currents underlying the AHP. Here, current-voltage relationships for  $Ca_v1.2$  mediated current have been generated in the absence and presence of 4R0N tau, using whole cell electrophysiology in tsA-201 cells. This demonstrated that 4R0N tau can significantly augment  $Ca_v1.2$  mediated current. It has been hypothesised that a direct interaction between 4R0N tau and  $Ca_v\beta$  is responsible for augmentation of  $Ca_v1.2$  mediated current. Here, mutants of 4R0N tau have been generated to identify residues involved in this interaction. It has been shown that mutation of residues in the second proline rich domain of tau (P155/P158) abolish the ability of 4R0N tau to augment  $Ca_v1.2$  mediated current. An excess of 4R0N tau and upregulation LTCCs has been reported in individuals with AD, as well as in aged animals experiencing cognitive decline. Therefore, resolution of the site on 4R0N-tau mediating augmentation of calcium current may open new avenues for therapeutics in the treatment of cognitive decline with age and in AD.

## **Author's declaration**

I declare that the work in this dissertation was carried out in accordance with the requirements of the University's Regulations and Code of Practice for Research Degree Programmes and that it has not been submitted for any other academic award. Except where indicated by specific reference in the text, the work is the candidate's own work. Work done in collaboration with, or with the assistance of, others, is indicated as such. Any views expressed in the dissertation are those of the author.

SIGNED: Emily Withers

DATE: 02/04/2023

## List of Abbreviations

<sup>166-172</sup>~~4R0N tau~~: 4R0N tau with residues <sup>166</sup>KKVAVVR<sup>172</sup> deleted

**AD**: Alzheimer's Disease

**AHP**: Afterhyperpolarisation

**AID**: Alpha interaction domain

**CaM**: Calmodulin

**CDI**: Calcium dependent inactivation

**Co-IP**: Co-immunoprecipitate

**Cryo-EM**: Cryogenic electron microscopy

**CSF**: Cerebrospinal fluid

**DHP's**: Dihydropyridines

**eGFP**: Enhanced green fluorescent protein

**FRET**: Fluorescence resonance energy transfer

**GK Domain**: Guanylate kinase-like Domain

**HEK293 cells**: Human embryonic kidney 293 cells

**HVA**: High Voltage Activated

**I<sub>mAHP</sub>**: Currents underlying medium AHP

**I<sub>sAHP</sub>**: Currents underlying slow AHP

**L-LTP**: LTP establishment phase

**LTCC's**: L – Type Calcium Channels

**LTD**: Long-term depression

**LTP**: Long-term potentiation

**MAPT**: Tau gene

**NMDAR**: N-methyl-D-aspartate receptor

**PCR**: Polymerase chain reaction

**PD**: Pore domain

**PP155/8AA 4R0N tau**: 4R0N tau with residues P155 and P158 mutated to alanine

**SH3 Domain:** SRC Homology 3 Domain

**SK:** Small conductance calcium-activated potassium

**TMS:** Transcranial magnetic stimulation

**tsA-201 cells:** Large T-antigen transformed HEK293 cells

**VDI:** Voltage dependent inactivation

**VGCC's:** Voltage – Gated Calcium Channels

**Vrev:** Reversal potential

**VSD:** Voltage sensor domain

## List of Figures

<b>Figure 1.1:</b> Structure of a voltage gated calcium channel.....	<b>13</b>
<b>Figure 1.2:</b> Structure of the $\alpha_1$ pore forming subunit of a VGCC.....	<b>14</b>
<b>Figure 1.3:</b> NMR modelling of the $\text{Ca}_v\beta$ subunit bound to the $\text{Ca}_v\alpha_1$ subunit.....	<b>16</b>
<b>Figure 1.4:</b> Application of Isradipine, a selective L-type channel blocker, leads to a concentration dependent reduction in currents underlying the medium and slow AHP.....	<b>18</b>
<b>Figure 1.5:</b> Nimodipine enhances the firing rate of pyramidal hippocampal neurones in rabbits.....	<b>20</b>
<b>Figure 1.6:</b> Structure of the six tau isoforms.....	<b>21</b>
<b>Figure 1.7:</b> Recordings of the currents underlying the sAHP and mAHP in hippocampal neurones.....	<b>23</b>
<b>Figure 1.8:</b> Current voltage relationships for $\text{Ca}_v1.2$ and $\text{Ca}_v1.3$ in tsA-201 cells in the presence of 4R0N tau.....	<b>24</b>
<b>Figure 2.3.1:</b> Transfection of tsA-201 cells with $\text{Ca}_v1.2$ has a lower efficacy than $\text{Ca}_v1.3$ ...	<b>30</b>
<b>Figure 2.3.2:</b> There is no notable difference in transfection efficacy of $\text{Ca}_v1.2$ expressed in PIRE5 vs PCDNA 3.1 in tsA-201 cells.....	<b>34</b>
<b>Figure 2.3.3:</b> A 24-hour low temperature incubation step increases current size without effecting the activation kinetics of the channel.....	<b>36</b>
<b>Figure 2.5.1:</b> Primers for deletion mutation.....	<b>37</b>
<b>Figure 2.5.2:</b> Primers for proline to alanine mutations.....	<b>38</b>
<b>Figure 2.6.1:</b> Voltage step protocol.....	<b>40</b>
<b>Figure 3.1.1</b> LTCC state transitions.....	<b>44</b>
<b>Figure 3.1.2:</b> Structure of a DHP agonist and antagonist.....	<b>47</b>
<b>Figure 3.1.3:</b> DHP binding regions on the $\alpha_1$ pore forming subunit of LTCC's.....	<b>47</b>
<b>Figure 3.2.1:</b> tsA-201 cells are devoid of endogenous calcium current.....	<b>48</b>
<b>Figure 3.2.2:</b> Expressed $\text{Ca}_v1.2$ and $\text{Ca}_v1.3$ have distinct current-voltage relationships in tsA-201 cells.....	<b>49</b>



<b>Figure 3.2.3:</b> Application of 10 $\mu$ M nimodipine markedly decreases Ca <sub>v</sub> 1.2 macroscopic current in tsA-201 cells expressing Ca <sub>v</sub> 1.2 and 4R0N tau.....	<b>51</b>
<b>Figure 4.2.1:</b> Co-expression of 4R0N tau in tsA-201 cells results in augmentation of macroscopic Ca <sub>v</sub> 1.2 current, without changing activation kinetics.....	<b>58</b>
<b>Figure 4.2.2:</b> Co-expression of 4R0N tau in tsA-201 cells causes an increase in macroscopic Ca <sub>v</sub> 1.2 current, without changing any channel kinetics (low temperature incubation) .....	<b>60</b>
<b>Figure 5.1.1:</b> Structure of tau filaments in various tauopathies.....	<b>66</b>
<b>Figure 5.1.2:</b> Structure of 4R2N tau.....	<b>67</b>
<b>Figure 5.1.3:</b> Amino acid sequences of 4R2N and 4R0N tau for deletion mutation.....	<b>68</b>
<b>Figure 5.1.4:</b> Crystal structure of Ca <sub>v</sub> $\beta$ <sub>3</sub> .....	<b>70</b>
<b>Figure 5.1.5:</b> Ca <sub>v</sub> $\beta$ <sub>3</sub> binds more strongly to 4R0N tau than 4R1N tau in co-IP assays using tau antibody.....	<b>71</b>
<b>Figure 5.1.6:</b> Amino acid sequences of 4R2N and 4R0N tau for substitution mutation.....	<b>73</b>
<b>Figure 5.2.1:</b> <sup>166-172</sup> del 4R0N tau can augment macroscopic Ca <sub>v</sub> 1.2 current in tsA-201 cells, to the same extent as WT 4R0N tau.....	<b>75</b>
<b>Figure 5.2.2:</b> Mutation of prolines 155 and 158 to alanine abolishes 4R0N tau augmentation of macroscopic calcium current in tsA-201 cells, without changing activation kinetics.....	<b>77</b>
<b>Figure 5.2.3:</b> Residues P155/P158 and KKVAVVR are both located in the second proline rich domain of 4R0N tau.....	<b>80</b>

## List of Tables

<b>Table 1.1:</b> Classification and properties of VGCC's.....	<b>12</b>
<b>Table 2.3.1:</b> Transfection conditions for each experimental group.....	<b>28</b>
<b>Table 2.3.2:</b> PCR mixture for a total reaction volume of 50 $\mu$ l.....	<b>31</b>
<b>Table 2.3.3:</b> PCR settings for KOD Hot Start and Stratagene Quikchange II XL kit.....	<b>34</b>
<b>Table 2.3.4:</b> Reaction mixtures for cutting PCR product and plasmid at Not1 and Kpn1 sites.....	<b>33</b>
<b>Table 2.3.5:</b> Reaction mixtures for a test and control ligation reaction.....	<b>33</b>
<b>Table 2.3.6:</b> Timeline of protocol between transfection and electrophysiology, with and without low temperature incubation.....	<b>35</b>
<b>Table 2.5.1:</b> PCR reaction for mutagenesis.....	<b>39</b>

# Table of Contents

<b>1. Introduction.....</b>	<b>12</b>
1.1 Structure and Classification of L-type Calcium Channels .....	12
1.2 Role of Auxillary Subunits.....	15
1.3 Age Related Changes in LTCC's in Neurones .....	17
1.4 Tau.....	21
1.5 Effect of Tau on LTCC Function .....	23
1.6 Hypothesis and Aims:.....	25
<b>2. Methods.....</b>	<b>27</b>
2.1 Cell Line .....	27
2.2 Maintenance of Cell Line .....	27
2.3.1 Transfection Method.....	28
2.3.2 Transfection of Ca <sub>v</sub> 1.2 in tSA-201 Cells has a Lower .....	30
2.3.3 Cloning .....	32
2.3.4 Ca <sub>v</sub> 1.2 Transfection Efficiency is Not Improved by Subcloning into PCDNA 3.1 .....	35
2.3.5: Transfection Using Low Temperature Incubation.....	35
2.4 Preparations of Plasmids .....	37
2.5 Mutagenesis .....	38
2.6 Electrophysiology.....	40
2.7 Data Analysis .....	41
<b>3. Characterisation of Expressed LTCC's in tsA-201 Cells .....</b>	<b>44</b>
3.1 Introduction .....	44
3.1.1 tsA-201 Cells .....	44
3.1.2 Kinetics of Ca <sub>v</sub> 1.2 and Ca <sub>v</sub> 1.3 .....	45
3.2.3 Pharmacology of Ca <sub>v</sub> 1.2 and Ca <sub>v</sub> 1.3 .....	47
3.2.1 Untransfected tSA-201 Cells are Devoid of Voltage – Gated Calcium Currents .....	49
3.2.2 Ca <sub>v</sub> 1.2 and Ca <sub>v</sub> 1.3 Display Distinct Current – Voltage Relationships.....	50
3.3.3 Nimodipine substantially blocks Ca <sub>v</sub> 1.2 mediated current at a Concentration of 10µM .....	51
<b>4. Tau Augmentation of LTCC Current.....</b>	<b>55</b>
4.1 Introduction .....	55
4.1.1 Increased LTCC Current and Cognitive Decline .....	55
4.1.2 Tau as a Potential Cause of LTCC Current Increase .....	56
4.2 Results .....	57
4.2.1 Co-expression of 4R0N Tau with Ca <sub>v</sub> 1.2 (β <sub>3</sub> , α <sub>2</sub> δ <sub>1</sub> ) Causes a Significant Increase in Calcium Current Amplitude .....	57
<b>5. Mutagenesis of Tau.....</b>	<b>65</b>
5.1 Introduction .....	65
5.1.1 Structure of Tau .....	65
5.1.2 The <sup>166</sup> KKVAVVR <sup>172</sup> region of tau: Influences on structure .....	67
5.1.3 Tau's Proline Rich Domains: Influences on structure and binding .....	70
5.2 Results .....	75
5.2.1 Deletion of region <sup>166</sup> KKVAVVR <sup>172</sup> does not diminish current augmentation .....	75

5.2.2 P155A/P158A Mutations Abolish Tau's Ability to Augment Current .....	77
5.3 Discussion .....	80
6. <i>Future Work</i> .....	85
7. <i>Conclusion</i> .....	87

# 1. Introduction

## 1.1 Structure and Classification of L-type Calcium Channels

Voltage-gated calcium channels (VGCC's) are calcium selective transmembrane channels that are grouped into 5 classes, as shown in Table 1.1 (Catterall, 2011). They are localised in a wide variety of tissues throughout the body and are key in initiating physiological events from changes in membrane potential; via an influx of calcium into a cell (Zamponi et al., 2015). Such events range from muscle contraction to neuronal communication and even gene expression (Catterall, 2011).

The first evidence that calcium permeable channels existed on cell membranes was found in crustacean muscle cells in 1953 (Fatt and Katz 1953). Following this, investigation in rat and chicken sensory neurones indicated that there is distinct high voltage activated (HVA) and low voltage activated (LVA) components underlying calcium influx into a cell (Carbone and Lux, 1984). This is now known to be due to the varied electrophysiological properties of the voltage – gated calcium channel subtypes, some of which are localised in the same cell types.

L-type calcium channels (LTCC's) are the largest class of VGCC, they are high voltage activated (HVA) and known to produce long lasting currents. What enabled the classification of these channels was their sensitivity to dihydropyridines (DHP's) (Dolphin, 2006). BayK 8644 is a DHP agonist which enhances the open probability of LTCC's, but not other VGCC's. DHP antagonists such as nimodipine promote the inactivated form of the channel and can be used to isolate the currents produced by

LTCC's in tissues (Hess, Lansman, Tsien, 1984). These currents were found in the heart, smooth muscle, skeletal muscle and in neurones.

Ca <sup>2+</sup> Current Type	Genes for $\alpha_1$ Subunits	Main Functions	Pharmacology	Kinetics
L	Ca <sub>v</sub> 1.1	Skeletal muscle voltage sensor	DHP sensitive	Activates at +7mV Slow inactivation
	Ca <sub>v</sub> 1.2	Cardiac/smooth muscle function Neuronal excitability	DHP sensitive	Activates at -30mV Slow inactivation
	Ca <sub>v</sub> 1.3	Hearing, sino-atrial node function Neuronal excitability	DHP sensitive	Activates at -55mV Slow inactivation
	Ca <sub>v</sub> 1.4	Retinal neurotransmission	DHP sensitive	Activates at -40mV Slow inactivation
N	Ca <sub>v</sub> 2.1	Synaptic transmission in the CNS	$\omega$ -CTx-GVIA sensitive	Activate at -20mV, partial inactivation
P/Q	Ca <sub>v</sub> 2.2	Synaptic transmission in the PNS	$\omega$ -Agatoxin sensitive	Activate at -20mV, partial inactivation
R	Ca <sub>v</sub> 2.3	Present in some neurones and synapses	SNX-482 sensitive	Activate at -20mV, partial inactivation
T	Ca <sub>v</sub> 3.1, 3.2 and 3.3	Neuronal excitability, pacemaker activity, subthreshold oscillations	Mibefradil sensitive	Activate at -70mV Rapid inactivation

**Table 1.1. Classification and properties of VGCC's.** (Adapted from Dolphin, 2018; Caterall, 2011; Clozel, Ertel and Ertel, 1997; Lipscombe, Helton and Xu, 2004; Feng, Kalyaanamoorthy and Barakat, 2018; Hille, 1992).

The sensitivity of LTCC's to DHP's was also key in fully understanding their structure (Dolphin, 2006). The skeletal muscle calcium channel (known as the DHP receptor complex) was the first to be purified. It was found to consist of  $\alpha_1$ ,  $\alpha_2\delta$ ,  $\beta$  and  $\gamma$  subunits interacting with a 1:1 stoichiometry. This isolation of individual subunits led to the cloning of DHP receptors from other tissue, allowing for the identification of all LTCC subtypes. These channels, like all VGCC's are composed of an  $\alpha_1$  pore forming subunit and 2/3 auxiliary subunits, which are coded for by separate genes, as shown in Figure 1.1 (Simms and Zamponi, 2012). The  $\alpha_1$  subunit determines the identity of the channel, whereas the auxiliary subunits have a regulatory role.

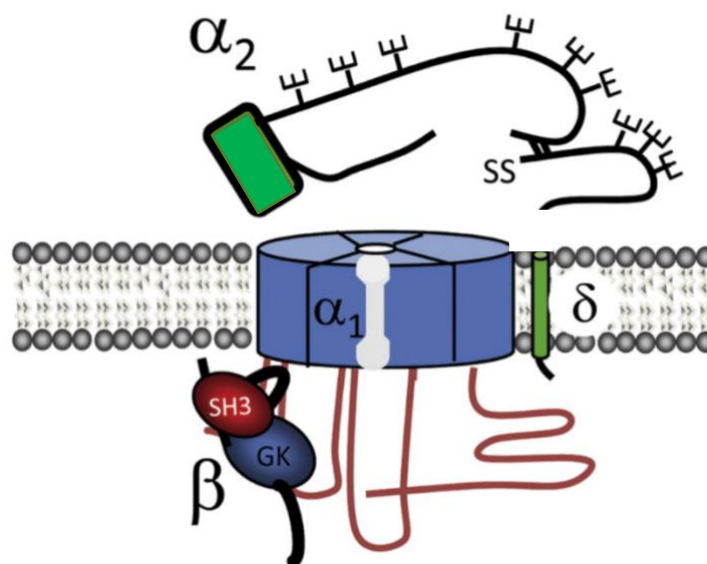


**Figure 1.1. Structure of a voltage gated calcium channel.** The  $\alpha_1$  pore forming subunit allows influx of calcium into a cell. The  $\beta$  subunit binds to the  $\alpha_1$  subunit at the intracellular side of the plasma membrane and contains a putative SRC Homology 3 (SH<sub>3</sub>) domain and a guanylate kinase-like (GK) domain. The  $\alpha_2\delta$  subunit traverses the membrane and extends into the extracellular matrix where it is highly glycosylated. (Simms and Zamponi, 2012).

As illustrated in Figure 1.2, the  $\alpha_1$  pore forming subunit is made up of 4 repeats, each comprised of six transmembrane segments (Neely and Hidalgo, 2014). To sense changes in membrane potential, there are several arginine and lysine residues on the fourth transmembrane segment (S4) of each repeat (Dolphin, 2006). Any conformational change that occurs in the voltage sensor, in response to voltage, leads to a change in conformation of the pore domain, allowing ions to pass through.

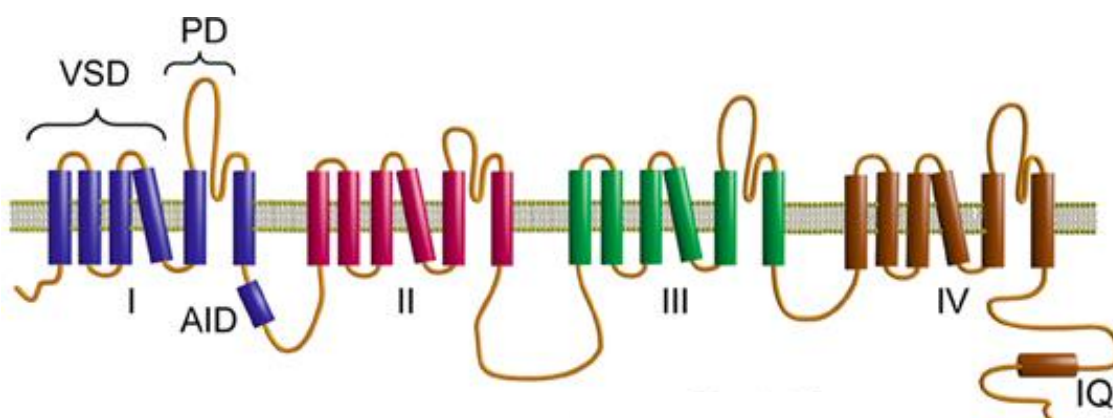


**Figure 1.2: Structure of the  $\alpha_1$  pore forming subunit of a VGCC.** Each repeat contains a pore domain (PD) between S5 and S6 and a voltage sensor domain (VSD) comprised of S1 – S4. The alpha interaction domain (AID) forms a binding site for the  $\beta$  subunit and the IQ domain binds  $\text{Ca}^{2+}$ /calmodulin. (Neely and Hidalgo, 2014).

## 1.2 Role of Auxillary Subunits

Auxillary subunits are proteins which are non-covalently bound to the pore forming  $\alpha_1$  subunit, as depicted in Figure 1.1 (Campiglio and Flucher, 2015). The canonical auxillary subunits are  $\beta$ ,  $\alpha_2\delta$ , and  $\gamma$ , with the  $\gamma$  subunit only known to be expressed with pore forming subunits in skeletal muscle (Yang et al., 2011).



The  $\alpha_2\delta$  subunits can be expressed as  $\alpha_2\delta_1 - \alpha_2\delta_4$  (Campiglio and Flucher, 2015). The variants are encoded for by 4 separate genes, with the  $\alpha_2\delta$  complex cleaved into separate polypeptides then joined by disulphide bonds (Dolphin, 2013). As shown in Figure 1.1 the  $\delta$  polypeptide traverses the membrane while the  $\alpha_2$  polypeptide is extracellular, but anchored to the membrane via its C-terminus (Geisler, Schopf and Obermair, 2014). The  $\alpha_2$  polypeptide extends into the cellular matrix and is highly glycosylated (Simms and Zamponi, 2012). The  $\alpha_2\delta$  subunit appears to have roles in the targeting the  $Ca_v1.2$  complex to appropriate locations at the cell membrane and, once there, it is involved in anchoring  $Ca_v1.2$  to the membrane and stabilising the complex (Dolphin, 2013). It may also affect the gating properties of the channel. For example, in heterologous systems, expression of  $\alpha_2\delta$  with  $\alpha_1$  results in an increased expression of functional channels at the cell membrane (Shistik et al., 1995).

There are 4 isoforms of the  $\beta$  subunit ( $\beta_{1-4}$ ) which are encoded for by separate genes (Campiglio and Flucher, 2015). It binds the  $\alpha_1$  pore forming subunit at a cytoplasmic loop between repeats I and II, known as the AID, as shown in Figure 1.3 (Pragnell et al., 1994). The  $\beta$  subunit contains conserved GK and SH<sub>3</sub> domains, however the N/C terminus and the HOOK region are non - conserved (Campiglio and Flucher, 2015). The HOOK region forms a bridge between  $\beta_4$  and  $\beta_5$  strands of the SH<sub>3</sub> domain, and varies with length and amino acid sequence between isoforms (Buraei and Yang, 2010). Expression of the  $\beta$  subunit with the  $\alpha_1$  subunit in heterologous systems increases macroscopic current amplitude, by increasing the amount of  $\alpha_1$  subunit at the cell membrane. It is thought to be crucial for expression of functional VGCC's. This is hypothesised to be due to the  $\beta$  subunit occluding regions of  $Ca_v\alpha_1$  on binding, causing a shift in the balance of endoplasmic reticulum retention and export

signals on the  $\alpha_1$  subunit (Fang and Colecraft, 2011). Expression of the  $\beta$  subunit has also been shown to induce a leftward shift in the voltage dependence of activation (Campiglio and Flucher, 2015).

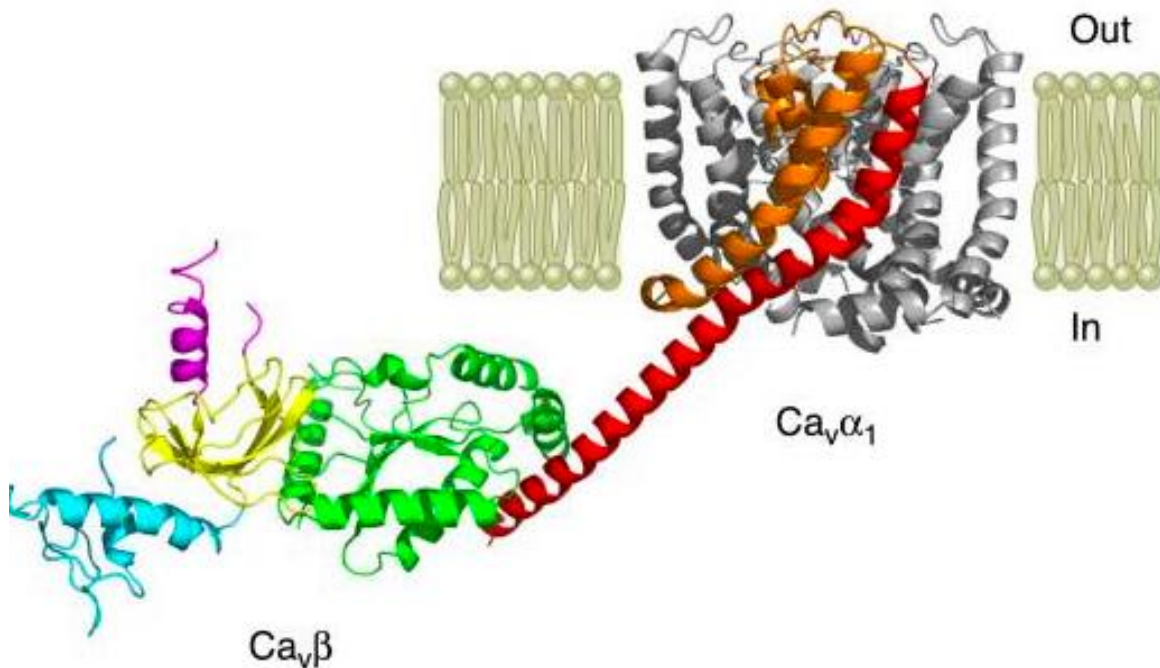


**Figure 1.3: NMR modelling of the  $\text{Ca}_v\beta$  subunit bound to the  $\text{Ca}_v\alpha_1$  subunit.** This image depicts the N-terminus (blue), SH3 domain (yellow), GK domain (green), HOOK region (purple) of the  $\beta$  subunit, alongside the S5 (orange) and S6 (red) of the  $\alpha_1$  subunit. The  $\beta$  subunit is binding at the AID (Buraei and Yang, 2010).

### 1.3 Age Related Changes in LTCC's in Neurones

LTCC's are expressed in a wide variety of tissues, although  $\text{Ca}_v1.2$  and  $\text{Ca}_v1.3$  are the only subtypes found in the brain (Zamponi et al., 2015). These channels are primarily located on the soma and dendritic spines of post-synaptic neurones; however, their subcellular distribution is distinct (Zhang et al., 2006). These channels are involved in long term potentiation (LTP), the process of learning and memory in

the brain, as well as in modulating the rate of neuronal firing (Striessnig and Koschak, 2008; Disterhoft et al., 1996).

LTP is the main form of synaptic plasticity thought to be the mechanism by which people can learn and acquire new memories (Bliss et al., 2018). It involves an initiation phase which is characterised by an increase in the trafficking of calcium permeable AMPA receptors to the cell membrane, and an establishment phase (L-LTP) in which changes in gene expression and synthesis of new proteins enables the increase in synaptic strength to be maintained over long periods of time. Studies in genetically modified mice have found that hippocampal function, including L-LTP, is dependent largely on Cav1.2 (Striessnig and Koschak, 2008). Furthermore, increase in calcium conductance via VGCC's in aged neurones has been observed alongside deficits in LTP (Burke and Barnes, 2006). Other biophysical properties which influence LTP, such as resting membrane potential and action potential threshold, remained the same. This makes the increase in calcium conductance the likely candidate for the LTP deficits observed. In terms of the underlying mechanism, it has been proposed that postsynaptic Cav1.2/1.3 are involved in setting a 'threshold' for LTP or long-term depression (LTD). Animal data supports this hypothesis. For example, It was found that aged rats, which were known to be subject to calcium dysregulation, were more susceptible to reversal of LTP (Norris, Korol and Foster, 1996).

Cav1.2 may have a further, more acute, role in learning and memory due to the influence of Cav1.2 currents on the duration of afterhyperpolarisations (AHP's) (Lima and Marrion, 2007). AHPs drive the cell's membrane potential below the normal

resting potential and contribute to the refractory period between action potentials (Burdyga and Wray, 2005). There are three types of AHP: fast, medium and slow, which are initiated at the onset of a burst, over hundreds of milliseconds, and over seconds respectively (Storm, 1987; Lancaster & Adams, 1986; Stocker, Krause and Pedarzani, 1999). Despite there being some debate surrounding the source of the currents underlying AHP's, it is widely accepted that both the medium and slow AHPs require  $\text{Ca}^{2+}$  entry via L- type calcium channels, as demonstrated by Figure 1.4 (Lima and Marrion, 2007).

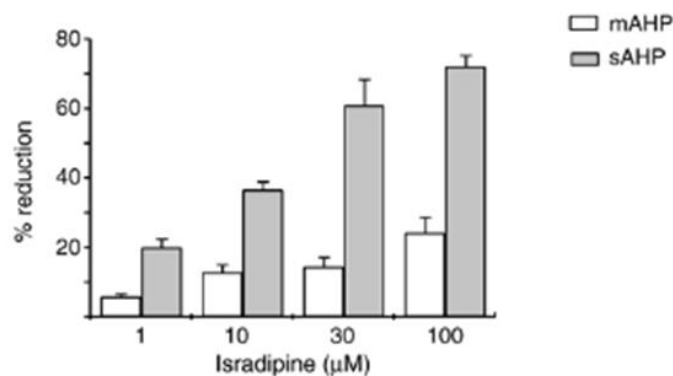


**Figure 1.4: Application of Isradipine, a selective L-type channel blocker, leads to a concentration dependent reduction in currents underlying the medium and slow AHP ( $I_{\text{mAHP}}/I_{\text{sAHP}}$ ).** This effect is larger for the  $I_{\text{sAHP}}$  with 100 $\mu\text{M}$  Isradipine resulting in a 72% reduction in  $I_{\text{sAHP}}$  and only a 25% reduction in  $I_{\text{mAHP}}$ . Graph shows mean data (n=3-8 depending on condition) with SEM (Lima and Marrion, 2007).

The influence of L-type calcium channels on AHPs is significant due to the role of AHPs in regulating the firing rate of neurones, which in turn modulates cognition (Matthews, Linardakis and Disterhoft, 2009). If an AHP amplitude or duration is

augmented this causes a decrease in the intrinsic excitability of neurones, as they fire less frequently if the membrane is more hyperpolarised for longer periods of time. It is thought that age related cognitive decline is linked to changes in the intrinsic excitability of neurones, which has downstream effects on the induction of LTP and synaptogenesis. In support of this, it has been observed that the amplitude of the  $I_{sAHP}$  increases in hippocampal neurones of aged animals (Matthews, Linardakis and Disterhoft 2009; Disterhoft et al., 1996). This can be correlated with a decrease in neuronal excitability and impaired learning. Interestingly, as shown by Figure 1.4, inhibition of LTCC's by nimodipine reduced the amplitude of the  $I_{sAHP}$ , increased the neuronal firing rate and enabled aged animals to learn as effectively as young animals (Thompson, Deyo and Disterhoft, 1990). Taken together, this information suggests that the decline in cognition seen with normal aging is related to an increase in L-type calcium current in the hippocampus, resulting in an increase in the  $I_{sAHP}$  and a subsequent decrease in neuronal firing. In support of this, studies in aged rats have shown that there is a significantly increased expression of  $Ca_v1.2$  on the surface membrane of CA1 and CA3 hippocampal neurones, which would inevitably result in an increase in L-type calcium current in these regions (Núñez-Santana et al., 2014).

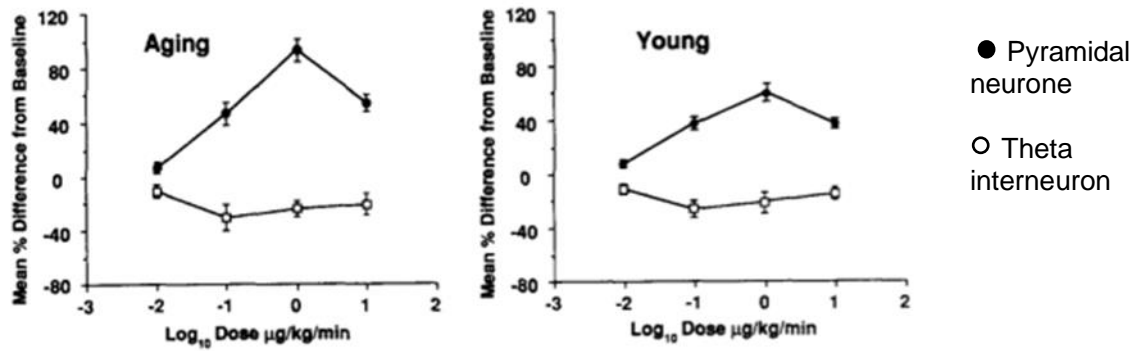


**Figure 1.5: Nimodipine enhances the firing rate of pyramidal hippocampal neurones in rabbits.** This effect was larger in aging animals which also had a larger amplitude  $I_{sAHP}$  and poorer baseline cognition than young animals. No effect was observed when recording from theta interneurons exposed to nimodipine. Graph displays mean values ( $n=13-31$  depending on group) with SEM (Thompson, Deyo and Disterhoft, 1990).

## 1.4 Tau

Tau is a microtubule associated protein with primary roles in microtubule assembly and stabilisation (Sotiropoulos et al., 2017). However, more recent research has demonstrated that tau localises to several other subcellular compartments and carries out diverse roles including regulating LTP, modulating vesicle release, and even maintaining the integrity of genomic DNA. Recently, overexpression of specific isoforms of tau has been shown to disrupt endocytic mechanisms and interfere with processing of amyloid (Mahendran et al., 2020).

In the human brain tau exists in 6 different isoforms due to alternative splicing of exons 2, 3 or 10 of the tau gene (MAPT) (Zhong et al., 2012). Consequently, the isoforms differ by the number of C-terminal repeats (3-4) and near-N terminal

repeats (0-2), as shown in Figure 1.6, but otherwise are conserved (Fichou et al., 2019). Tau is an intrinsically disordered protein, and therefore it has little tertiary structure. Having said this, recently cryogenic electron microscopy (cryo-EM) evidence has emerged suggesting that when arranged in filaments tau is able to fold into a variety of shapes, which appear to differ between disease states (Scheres et al., 2020).

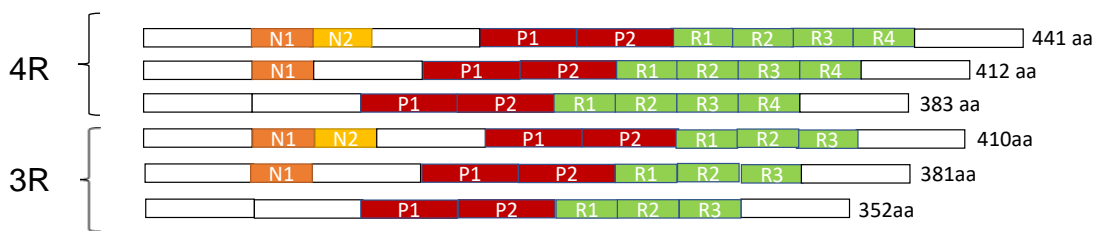


**Figure 1.6: Structure of the six tau isoforms.** Tau is a disordered protein with little tertiary structure. It consists of proline rich domains (P), 3/4 C-terminal repeats (R), and 0-2 near N-terminal repeats (N) (Adapted from Fichou et al., 2019).

Remarkably, the ratio of the different isoforms appears to shift with age and contributes to whether tau is behaving pathologically. Within normal ageing and in the brains of Alzheimer's Disease (AD) patients, it has been observed that the ratio of 4R to 3R tau increases in the midfrontal cortex and hippocampus, with 4R0N tau being the most abundant isoform (Yasojima, McGeer and McGeer, 1999; Kimur et al, 2016). AD is a sporadic, progressive neurodegenerative disorder characterised by a loss of executive function alongside memory, attentional and praxis deficits (Minati et al., 2009). AD accounts for 70% of all dementia and is characterised by neuronal cell loss, together with the presence of plaques containing amyloid beta and deposits of hyperphosphorylated tau (Kametani and Hasegawa., 2018). Interestingly there are areas in which the 3R isoforms still dominate in adulthood, such as the granule cells

in the dentate gyrus (Zhong et al., 2012). These resist aggregation, a phenomenon in which disordered proteins bind together, even in AD. This suggests that it is the presence of 4R isoforms which leads to the plaques of hyperphosphorylated tau. Having said this, research now suggests that it is not the aggregates of hyperphosphorylated tau that cause the disease but rather the soluble fragments that are present in abundance before this process occurs (Mroczko, Groblewska and Litman-Zawadzka). This makes the determining the pathology of AD even more challenging, as it is likely to be multifaceted when looking at the array of roles carried out by tau within a cell.

## 1.5 Effect of Tau on LTCC Function

Recent data have demonstrated that overexpression of 4R0N tau leads to augmentation of  $I_{CaV1.2}$  current and  $I_{sAHP} / I_{mAHP}$  as shown in Figure 1.7 (Stan et al., 2022). *In vitro* this would lead to a decrease in the rate of neuronal firing and therefore would replicate what has been observed in aged animals in previous studies (Núñez-Santana et al., 2014). This effect is more marginal for 4R2N tau whereas 4R1N tau did not cause any current augmentation.

When this is modelled in tsA-201 (large T-antigen transformed human embryonic kidney cells (HEK293)), 4R0N tau augmentation of  $I_{CaV1.2}$  mediated current appears to have both a  $\alpha$  and  $\beta$  subunit specificity. Tau appears to significantly augment current only when  $I_{CaV1.2}$  is expressed as the  $\alpha_1$  subunit and  $\beta_3$  is expressed as the  $\beta$  auxiliary, as shown in Figure 1.8.



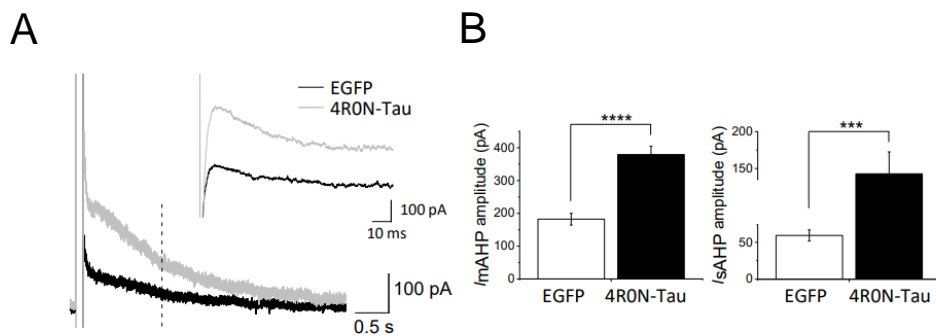


**Figure 1.7: Recordings of the currents underlying the sAHP and mAHP in**

**hippocampal neurones. A)** Example trace showing augmentation of currents

underlying the AHP with expression of 4R0N tau (sAHP in foreground) **B)** Bar charts showing mean current increase of currents underlying the sAHP and mAHP with overexpression of 4R0N tau (n=33-51, error bars show SEM) (Stan et al., 2022).

Similarly to what has been observed in aging animals (Núñez-Santana et al., 2014), non-stationary noise analysis revealed that the augmentation of calcium current, and so the AHP, was due to an increase in the number of LTCC's in the cell membrane. It is therefore an interesting possibility that age related cognitive decline begins due to an imbalance of 4R:3R tau, which causes a cascade of events that ultimately results in a decrease in neuronal excitability. The exact interactions between tau and the calcium channels are yet to be determined, but may be very significant in understanding the mechanisms underlying cognitive decline with ageing and in the early stages of AD.

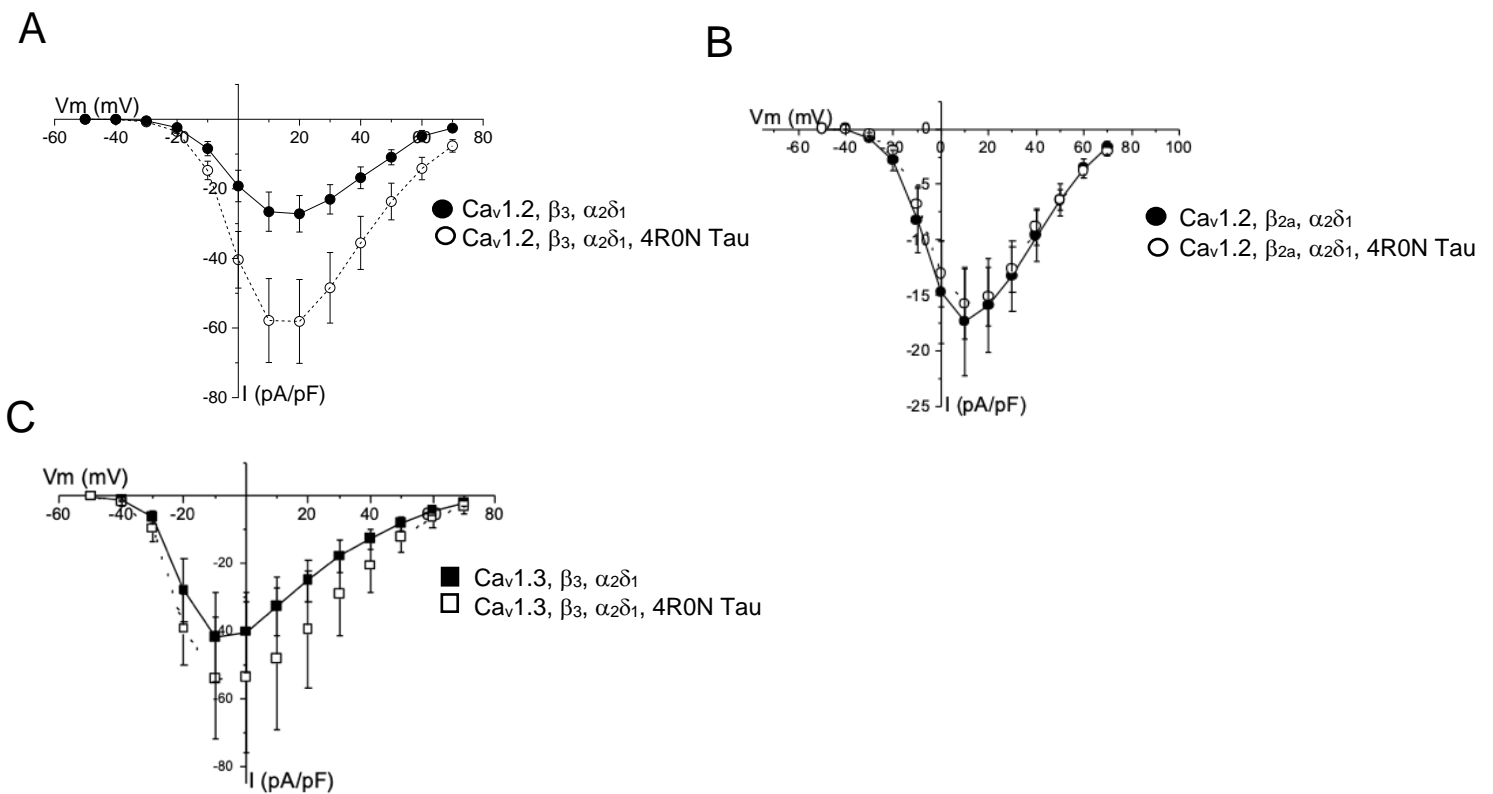


**Figure 1.8: Current voltage relationships for Cav1.2 and Cav1.3 in tsA-201 cells in the presence of 4R0N tau (Stan et al., 2022)** **A)** Tau significantly augments current when Cav $\beta_3$  is expressed with Cav1.2 (n=19 in each group) **B)** There is no current augmentation when tau is co-expressed with Cav $\beta_{2a}$  and Cav1.2 (n=6 in absence of tau, n=7 in presence of tau) **C)** There is a small, non-significant current augmentation when tau is co-expressed with  $\beta_3$  and Cav1.3 (n=8 in absence of tau, n=6 in presence of tau). Error bars show SEM.

## 1.6 Hypothesis and Aims:

The working hypothesis is that 4R0N tau augments Cav1.2 current by increasing the number of Cav1.2 channels at the cell membrane. This effect may involve 4R0N tau interacting with  $\beta_3$ , since  $\beta$  subunit specificity is observed.

The first aim of this investigation is to repeat the finding that tau increases LTCC current when co-expressed in tsA-201 cells with Cav1.2. I will then extend this analysis to assess whether tau is able to slow the decay of calcium current, to establish if this is one of the mechanisms by which it causes current augmentation. The second aim is to identify a region where 4R0N tau is interacting with Cav1.2.

## **2. Methods**

### **2.1 Cell Line**

The cell line chosen for this study was tsA-201. They are a commonly used mammalian cell line which are useful for electrophysiological studies, due to their morphology enabling easy voltage clamping and their ability to efficiently express recombinant proteins (Davies et al, 2006; Hulme et al., 2006). All cells were stored in liquid nitrogen, thawed using a 37°C water bath and seeded in 25cm<sup>2</sup> flasks containing 8ml DMEM+ (DMEM supplemented with 10% foetal bovine serum and 1% PenStrep (10,000 units/ml penicillin, 10,000µg/ml Streptomycin)).

### **2.2 Maintenance of Cell Line**

Cells were kept in an incubator at 37°C and 5% CO<sub>2</sub>. They were passaged when they reached 90% confluency, once or twice per week. To passage the cells DMEM+ was removed before washing in 2ml PBS; a balanced salt solution used to wash the cells and remove old media/dead cells. To detach cells from the base of the flask they were incubated in 2ml PBS based enzyme free cell dissociation buffer at 37°C for 4 minutes. The buffer is calcium free, disrupting the interactions between the cells and between the cell and the flask and causing them to lift off the bottom of the dish and detach from one another (Freshney, 2005). Once dissociated, 6ml DMEM+ was added and the cells triturated with a stripette to break up clumps, before seeding into a new flask at various diluted concentrations. All cell culture procedures were carried out in aseptic conditions inside a laminar-flow hood.

## 2.3 Transfection

### 2.3.1 Transfection Method

Cells were transfected using Lipofectamine 2000, a polycationic lipid able to deliver DNA to the nucleus (Dalby et al., 2004). The lipofectamine forms a lipoplex with the DNA molecules which passes through the cell membrane in an endosome. Once inside the cell the lipoplex must also cross the nuclear membrane before the DNA can be transcribed. Cells were transfected when they reached approximately 90% confluency as this was found to lead to optimal expression. Two Eppendorf tubes were prepared and incubated at room temperature for 5 minutes before combining, one containing Opti-MEM and lipofectamine, and one containing Opti-mem and DNA. The DNA, lipofectamine and Opti-MEM were added in set ratios depending on cell density, as shown in Table 2.3.1. In each condition 4 plasmids were used to keep the plasmid number consistent. To achieve this aim 4R0N tau was expressed on a bisstronic vector with enhanced green fluorescent protein (eGFP) in the 4R0N tau group, whereas eGFP was expressed alone in the control.

Eppendorf tubes were combined and incubated at room temperature for 30 minutes. During this second incubation cells were washed in PBS and DMEM+ was refreshed. The transfection mix was added in a dropwise manner. During the process of transfection refinement, the cells were transfected in both 25cm<sup>2</sup> flasks and 30x10mm dishes, however reagents were always added at 1µg/15.3cm<sup>2</sup>. The current sizes and transfection efficacy were the same whether the transfection was in a dish or a flask, so data were combined.

After transfection, cells were incubated for 24 hours before plating in dishes (Falcon 35mm x 10mm Easy Grip TC-Treated) containing 2ml DMEM + for a minimum of 18 hours prior to electrophysiological recording. The cells remained in the dishes for patch-clamp studies.

<b>Group</b>	<b>DNA</b>	<b>Lipofectamine</b>
Control	1 $\mu$ g/15.3cm <sup>2</sup> Cav1.2 (PIRES), 1 $\mu$ g/15.3cm <sup>2</sup> Cav $\alpha$ 2 $\delta$ 1 (pcDNA 3.1+/hygro), 1 $\mu$ g/15.3cm <sup>2</sup> Cav $\beta$ 3 (pcDNA 3), 1 $\mu$ g/15cm <sup>2</sup> eGFP (pEGFP-C3)	2.5 $\mu$ l/1 $\mu$ g of DNA
4R0N Tau (WT or Mutants)	1 $\mu$ g/15.3cm <sup>2</sup> Cav1.2 (PIRES), 1 $\mu$ g/15.3cm <sup>2</sup> Cav $\alpha$ 2 $\delta$ 1 (pcDNA 3.1+/hygro), 1 $\mu$ g/15.3cm <sup>2</sup> Cav $\beta$ 3 (pcDNA 3), 1 $\mu$ g/15.3cm <sup>2</sup> tau-eGFP (PIRES-eGFP)	2.5 $\mu$ l/1 $\mu$ g of DNA
Cav1.3	1 $\mu$ g/15.3cm <sup>2</sup> Cav1.3 (pcDNA 3.1), 1 $\mu$ g/15.3cm <sup>2</sup> Cav $\alpha$ 2 $\delta$ 1 (pcDNA 3.1+/hygro), 1 $\mu$ g/15.3cm <sup>2</sup> Cav $\beta$ 3 (pcDNA 3), 1 $\mu$ g/15.3cm <sup>2</sup> eGFP (pEGFP-C3)	2.5 $\mu$ l/1 $\mu$ g of DNA

**Table 2.3.1: Transfection conditions for each experimental group.** Vectors for each DNA constructs are shown in brackets.

### **2.3.2 Transfection of Ca<sub>v</sub>1.2 in tSA-201 Cells has a Lower Efficacy than Transfection of Ca<sub>v</sub>1.3**

The method of transfection for this investigation was refined over several months. This process was initiated by the observation that Ca<sub>v</sub>1.3 had a higher transfection efficacy than Ca<sub>v</sub>1.2, as demonstrated by Figure 2.3.1. For the purpose of this study, transfection efficacy will be defined as the percentage of cells that were expressing LTCC's alongside eGFP, and the current density within these cells. A low transfection efficacy is problematic as if many cells are not expressing Ca<sub>v</sub>1.2, patch clamp becomes a very low throughput method, and resources are wasted on transfections. Additionally, if the current density is low then it can be difficult to distinguish signal from noise.

Due to the Cav1.2 and Cav1.3 plasmids being of very similar size, and the auxillary subunits in each transfection being the same, it seemed that the most likely factor causing this difference was the expression vector, with the Ca<sub>v</sub>1.3 being expressed in PCDNA 3.1 and the Ca<sub>v</sub>1.2 in a PIRE5. Consequently, it was important to assess whether cloning of the Ca<sub>v</sub>1.2 construct into PCDNA 3.1 enabled a higher transfection efficacy.

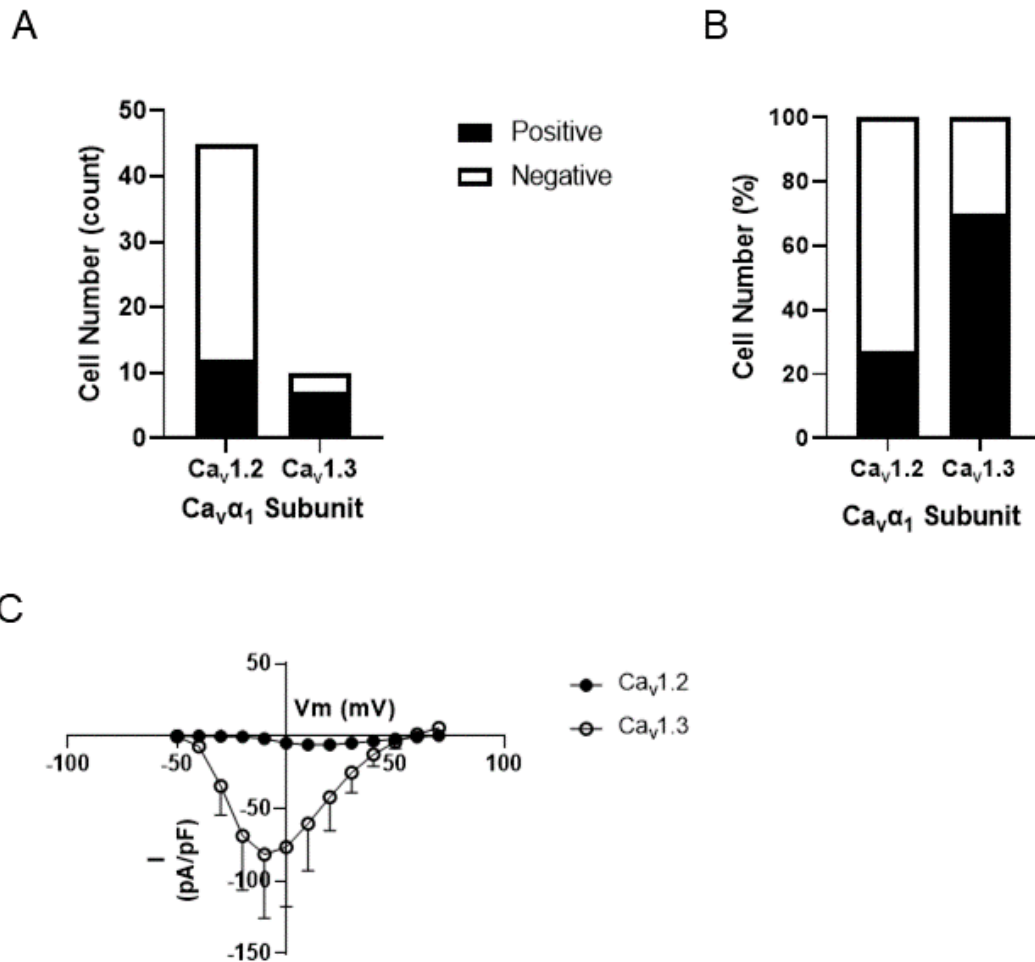


**Figure 2.3.1: Transfection of tSA-201 cells with Ca<sub>v</sub>1.2 has a lower efficacy than Ca<sub>v</sub>1.3** **A**) Percentage of cells expressing eGFP that also expressed functional calcium channel current when transfected with Ca<sub>v</sub>1.2 (n=45) or Ca<sub>v</sub>1.3 (n=12) **B**) Cell count showing the number of cells expressing functional calcium current when transfected with Ca<sub>v</sub>1.2 (n=45) or Ca<sub>v</sub>1.3 (n=12) **C**) IV curve showing calcium currents normalized to capacitance for Ca<sub>v</sub>1.2 (n=45) and Ca<sub>v</sub>1.3 (n=12). Currents were generated by 10mV step depolarisations, from -50mV to +70mV, from a holding potential of -80mV. Error bars show SEM.



### 2.3.3 Cloning

Cav1.2 was subcloned into the pcDNA 3.1(+) vector using polymerase chain reaction (PCR). Primers were designed to add restriction sites and a Kozak sequence to the template DNA. Restriction sites enable the gene of interest to be inserted into the new vector and the Kozak sequence enhances expression. Restriction sites must be selected that are in the new construct (i.e. pcDNA 3.1) but not in the cDNA you are cloning (i.e Cav1.2). Kpn1 was the restriction enzyme used at the 5' end and Not1 at the 3' end. PCR was set up using KOD Hot Start DNA Polymerase kit as shown in Table 2.3.2 and put in a PCR machine using the protocol in Table 2.3.3.

Component	Volume
10x Buffer for KOD Hot Start DNA Polymerase	5 $\mu$ l (final concentration = 1x)
25mM MgSO <sub>4</sub>	3 $\mu$ l
2mM dNTPs	5 $\mu$ l
dH <sub>2</sub> O	20.5 $\mu$ l
DMSO	2.5 $\mu$ l
Forward Primer (10 $\mu$ M)	Add 1.5 $\mu$ l
Reverse Primer (10 $\mu$ M)	Add 1.5 $\mu$ l
Template DNA (1ng/ $\mu$ l)	10 $\mu$ l
KOD Hot Start DNA Polymerase	1 $\mu$ l

**Table 2.3.2: PCR mixture for a total reaction volume of 50 $\mu$ l**

	<b>Step 1</b>	<b>Step 2</b>	<b>Step 3</b>	<b>Step 4</b>	<b>Step 5</b>	<b>Step 6</b>
KOD Hot Start Kit	95°C 2 minutes	95°C 20 seconds	60°C 10 seconds	70°C 3 minutes	GO TO STEP 2 X 24	10°C 5 minutes
Stratagene Quikchange II XL Kit	95°C 60 seconds	95°C 50 seconds	60°C 50 seconds	68°C 7 minutes	GO TO STEP 2 x 18	72°C 7 minutes

**Table 2.3.3: PCR settings for KOD Hot Start and Stratagene Quikchange II XL**

**kit**

Following this, gel electrophoresis was used to assess if the PCR had amplified the gene of interest. Agarose gels were prepared using TAE buffer (20mM tris, 10mM acetic acid, 0.5mM EDTA) containing 1% agarose, and microwaved until the agarose had dissolved. Following this ethidium bromide was added at a concentration of 0.5µg/ml and the gel poured into a mould. Once the gel was set 10µl of marker was put in the first lane, and DNA containing 1x dye in the following lanes. TAE buffer was added to cover the surface of the gel and the power switched on for 20 minutes, so that the cathode is near the wells and the anode at the opposite end of the gel (as DNA has a negative charge it will run to the anode). Once this was complete the gel was exposed to UV light and the DNA visualised.

When it is established that the PCR was successful, the DNA was purified using a 'QIAquick PCR Purification Kit' following standard protocol, and DNA eluted in 50µl dH<sub>2</sub>O. PCR products containing Cav1.2 were incubated with restriction enzymes for

2 hours at 37°C. The pcDNA 3.1 vector was incubated with the same restriction enzymes as shown in Table 2.3.4.

PCR Component	Plasmid
12.5µl PCR product	1µl Plasmid
10µl 10x Cutsmart Buffer	10µl 10x Cutsmart Buffer
73.5µl dH <sub>2</sub> O	83µl dH <sub>2</sub> O
2µl Not1	2µl Not1
2µl Kpn1	2µl Kpn1
	2µl CIP (prevents plasmid re-ligating to itself)

**Table 2.3.4: Reaction mixtures for cutting PCR product and plasmid at Not1 and Kpn1 sites**

Following this the PCR product and vector were cleaned again using the ‘QIAquick PCR Purification Kit’ and eluted into 25µl dH<sub>2</sub>O. Additionally, both the cut PCR product and the cut plasmid were run on a gel to ensure that the DNA was still present. Finally, the vector and insert DNA were ligated with ligase enzymes during a 30-minute incubation as shown in Table 2.3.5.

Insert & Primer	Control
0.5µl Plasmid from restriction digest	0.5µl Plasmid from restriction digest
1.5µl PCR product from restriction digest	1.5µl dH <sub>2</sub> O
2µl Ligase enzyme	2µl Ligase enzyme

**Table 2.3.5: Reaction mixtures for a test and control ligation reaction**

The DNA was then transformed following the plasmid preparation protocol in section 2.4.

### 2.3.4 $Ca_v1.2$ Transfection Efficiency is Not Improved by Subcloning into PCDNA 3.1

Surprisingly, subcloning of  $Ca_v1.2$  into PCDNA 3.1. does not improve the transfection efficacy in tsA-201 cells, as shown in Figure 2.3.2. For this reason, it is likely to be something related to the translation or trafficking of the  $Ca_v1.2$  subunit, rather than the plasmid in which it is contained, which is impacting the transfection efficacy.

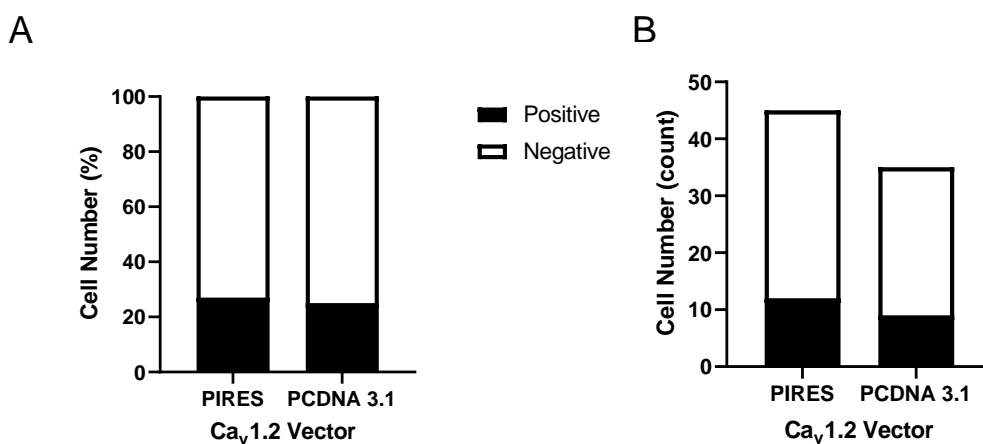


**Figure 2.3.2: There is no notable difference in transfection efficacy of  $Ca_v1.2$  expressed in PIRES vs PCDNA 3.1 in tsA-201 cells** **A)** Raw number of cells expressing  $Ca_v1.2$  in PIRES (n=45) or PCDNA 3.1 (n=35) **B)** Percentage of cells expressing  $Ca_v1.2$  in PIRES (n=45) or PCDNA 3.1 (n=35).

### 2.3.5: Transfection Using Low Temperature Incubation

The use of low temperature incubation to increase translocation of proteins to the cell membrane was first discovered as a means of rescuing of F508del-cystic fibrosis

transmembrane conductance regulator, the predominant cause of the genetic disorder cystic fibrosis (Denning et al., 1992). Therefore, to assess if this method was also able to increase the proportion of Cav1.2 at the cell membrane, a 24-hour 27°C incubation step was added to the protocol after the plating of transfected cells, as described in Table 2.3.6.

	Day 1	Day 2	Day 3	Day 4
No Incubation	Transfect	Plate cells (24 hour 37°C incubation)	Perform electrophysiological studies	
Low Temperature Incubation	Transfect	Plate cells (24 hour 37°C incubation)	Move into 27°C incubator for 24 hours	Perform electrophysiological studies

**Table 2.3.6: Timeline of protocol between transfection and electrophysiology, with and without low temperature incubation.**

The low temperature incubation markedly increased the success rate of transfection, and increases the current density (figure 2.3.3), making it easier to resolve the currents. Current was resolvable in over 90% the cells expressing eGFP. Therefore, for all investigations carried out past the point of the transfection method refinement, low temperature incubation will be used.

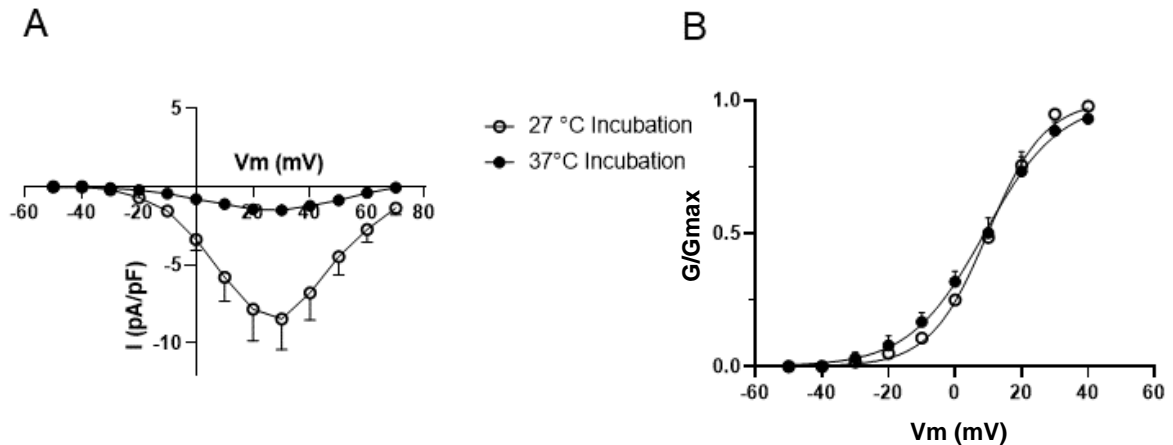


**Figure 2.3.3: A 24-hour low temperature incubation step increases current size without affecting the activation kinetics of the channel. A)** Current – voltage relationship for  $Ca_v1.2$ , with ( $n=6$ ) and without ( $n=8$ ) low temperature incubation step, generated by a voltage step protocol, from a holding potential of  $-80\text{mV}$  **B)** Activation curve for  $Ca_v1.2$  with and without low temperature incubation. Mean  $V_{1/2}$  for no low temperature incubation is  $9.8 \pm 0.67\text{mV}$  and mean slope is  $7.8 \pm 2.40\text{mV}$ , with low temperature incubation mean  $V_{1/2}$  is  $8.32 \pm 0.33\text{mV}$  and mean slope is  $9.90 \pm 1.12\text{mV}$ . There is no significant difference between  $V_{1/2}$  and slope when compared with an unpaired t – test ( $p>0.05$ ).

## 2.4 Preparations of Plasmids

All DNA was sequenced by Eurofins using Sanger Sequencing. To transform the DNA,  $DH5\alpha$  cells were thawed on ice and  $50\mu\text{l}$  of cells aliquoted into a prechilled  $1.5\text{ml}$  Eppendorf.  $10\text{ng}$  of DNA was added to the cells and gently mixed before incubating on ice for 30 mins. Next, cells were heat shocked for 20 seconds in a  $42^\circ\text{C}$  water bath followed by a 2-minute incubation on ice.  $950\mu\text{l}$  of prewarmed SOC

media was then added to each tube. 50µl and 150µl of the transformed mixture was spread onto separate LB plates containing 100µl/ml ampicillin. Plates were incubated overnight at 37°C. Single colonies were picked and incubated in LB medium containing ampicillin in a shaking incubator (225rpm) for 12-16 hours. Mini, midi and maxi preparations were made as needed using Qiagen Kits and following standard protocol.

## 2.5 Mutagenesis

Primers were designed by examining the sequence for 4R0N tau, as shown in figure 2.5.1/2.5.2. For the deletion mutations, primers were designed that consisted of the sequences flanking the deleted region; for the substitutions, primers were designed containing the desired substitution, and the flanking sequences.

### <sup>166</sup>KKVAVVR<sup>172</sup> Deletion:

**Forward 5'** CCAACCCCACCCACCCGGGAGCCCACTCCACCCAAGTCGCCGTCTTCC

**WT** CCAACCCCACCCACCCGGGAGCCC **AAGAAGGTGGCAGTGGTCCGT**ACT  
**4R0N Tau** CCACCCAAGTCGCCGTCTTC

**Reverse 5'** GGAAGACGGCGACTTGGGTGGAGTGGGCTCCCGGGTGGGTGGGGTTGG

Amino acid residues 496 – 516 deleted from 4R0N tau  
AAGAAGGTGGCAGTGGTCCGT = KKVAVVR

**Figure 2.5.1: Primers for deletion mutation.** Region highlighted in red shows the amino acid residues to be deleted from 4R0N tau sequence

**P155A:**

**Forward 5'** CCCGGCAGCCGCTCCCGCACC **GCG** TCCCTTCCAACCCCACCCA

**WT** CCCGGCAGCCGCTCCCGCACC **GCG** TCCCTTCCAACCCCACCCA  
**4R0N Tau**

**Reverse 5'** TGGGTGGGGTTGGAAGGGACGCGGTGCGGGAGCGGCTGCCGGG

Amino acid residue 463 swapped from cytosine to guanine  
CCG to GCG = Proline to alanine mutation

**P158A:**

**Forward 5'** CGCTCCCGCACC **GCG** TCCCTT **GCA** ACCCCACCCACCCGGGAGC

**P155A** CGCTCCCGCACC **CCG** TCCCTT **CCA** ACCCCACCCACCCGGGAGC  
**4R0N Tau**

**Reverse 5'** GCTCCCGGGTGGGTGGGGTTGCAAGGGACGCGGTGCGGGAGCG

Amino acid residue 472 swapped from cytosine to guanine  
GCA to CCA = Proline to alanine mutations

**2.5.2: Primers for proline to alanine mutations.** Regions highlighted in yellow and green show the amino acids to be substituted. In both cases, only one substitution (cytosine to guanine) was required. The substitutions were performed sequentially, therefore the first mutation is incorporated into the second primer

Mutations were carried out by PCR using the Stratagene Quikchange II XL kit. The PCR reaction mixture was set up as displayed in Table 2.5.1 and the PCR machine set to run as displayed in Table 2.3.3.



PCR Component	Amount
Reaction Buffer	5 $\mu$ l
Template DNA	1 $\mu$ l (10ng)
Forward Primer	1.25 $\mu$ l (125ng)
Reverse Primer	1.25 $\mu$ l (125ng)
dNTP	1 $\mu$ l
Quick Solution	3 $\mu$ l
dH <sub>2</sub> O	37.5 $\mu$ l
Polymerase	1 $\mu$ l

**Table 2.5.1: PCR reaction for mutagenesis.** The reaction mixture is a total of 50 $\mu$ l prior to adding polymerase, which should be added last and after mixing.

1 $\mu$ l of DpnI restriction enzyme was added to the PCR product and incubated for 1 hour at 37°C. Transformation was then carried out using 45 $\mu$ l of ultracompetent cells combined with 2 $\mu$ l of Beta-mercaptoethanol mix provided with the kit. Following this, the bacteria were incubated for 10 minutes on ice before adding 2 $\mu$ l of the DpnI treated DNA. Following this, normal transformation procedure was followed (section 2.4), with the heat shock extended to 30 seconds.

## 2.6 Electrophysiology

During electrophysiological recordings cells bathed in external solution (pH 7.4) at room temperature containing (mM): TEACl, 140; HEPES(acid), 10; CaCl<sub>2</sub>, 5; MgCl<sub>2</sub>, 1; D-glucose, 10. Macroscopic currents were recorded in the whole cell voltage clamp configuration using electrodes manufactured from borosilicate glass containing

internal solution (pH 7.4) (mM): CsMeSO<sub>3</sub>, 120; TEACl, 20; MgCl<sub>2</sub>, 2; MgATP, 4; HEPES(Na), 10; EGTA, 5. Internal solution was frozen and defrosted but kept on ice during recording. Electrodes were pulled using a Narishige PP-830 and polished to have a resistance of 2-4 Ω. Axopatch 200A was used to record current across the tSA-210 cell membrane via an ITC-16 interface (Instrutech Corp); filtering at a cut-off frequency of 1 kHz, using a Bessel filter, and sampling at a rate of 10 kHz. Step depolarisations, as shown in figure 2.6.1 were used to evoke current. Series resistance compensation was 80-90% throughout. All currents were normalised to cell capacitance for data analysis. The mean value for capacitance of cells expressing Cav1.2 in absence of tau was 16.1pF (n=12), and in presence of tau was 19.0pF (n=12).

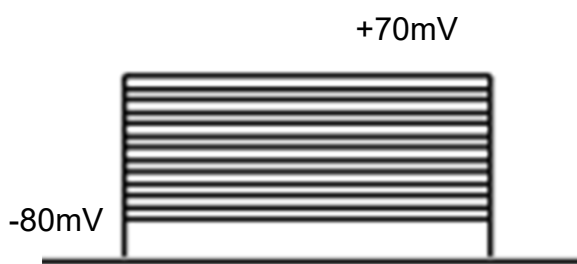


**Figure 2.6.1: Voltage step protocol.** Current

evoked by step depolarisations from a holding potential of -80mV, starting at -50mV then increasing by 10mV up to +70mV

## 2.7 Data Analysis

IV curves were generated by measuring the peak current amplitude at each voltage step using Pulse 8.8, then inputting these data into Excel. The data were plotted as membrane potential against current density in Prism 9. Absolute current size was converted into current density using the following equation:

$$\text{Current Density (pA/pF)} = \text{Current (pA)} / \text{Cell Capacitance (pF)}$$

Statistical significance between current voltage relationships in each experimental group was established by a two-way ANOVA with multiple comparisons. This is because there are two variables (voltage and tau), and always at least one variable with more than two groups (voltage and tau when it is a 3 way comparison).

Activation curves were generated by finding the conductance. This was calculated from peak current amplitude, assuming a reversal potential ( $V_{rev}$ ) of +70mV:

$$G = I/(V - V_{rev})$$

The conductance at each point of the voltage curve is then normalised and plotted against voltage. Conductance was only calculated in the range of -50mV to +40mV as above this voltage range an outward current is sometimes observed during the pulse, which would confound the results. Curves were plotted in Prism, but  $V_{1/2}$  and slope calculated in Origin. Unpaired t-tests were used to assess if there was a significant difference between  $V_{1/2}$  and slope between 2 groups, and one way ANOVA used to assess these differences between 3 groups.

To examine the rate of current decay an exponential was fit to currents generated by steps 0, +10, +20 and +30 mV because these points gave the best resolution of inward current. Currents were fitted with a single exponential. When trialled using two exponentials the value of current decay was inconsistent between cells and sometimes longer than the duration of the pulse itself. This is likely due to the low resolution of certain currents, but for this reason the analysis was more robust using one exponential. The rate of current decay in seconds for each voltage step was

plotted against voltage in Prism 9. Two-way ANOVA was used to establish any statistically significant difference between groups.

## 3. Characterisation of Expressed LTCC's in tsA-201 Cells

### 3.1 Introduction

#### 3.1.1 tsA-201 Cells

TsA-201 cells are HEK293 cells modified to express a SV40 T antigen, to enhance their ability to express recombinant proteins with an SV40 enhancer element (Park, Begenisich and Melvin, 2001). Human embryonic kidney 239 (HEK293) cells are produced by exposure of human embryonic kidney cells to fragments of DNA from human adenovirus type 5 (Thomas and Smart, 2005). These cells are useful for studies that involve expression of recombinant channels as they lack many ion channels of interest endogenously, while containing the proteins required to express and translocate these channels to the cell membrane, when they are transiently expressed (Stan et al., 2022). To confidently use a cell line to model an interaction in neurones, it is first important to establish that the heterologous system is appropriate, as will be confirmed within this section. As stated in section 1.5, the initial effect of tau on the sAHP and mAHP was observed in hippocampal neurones. Following this, the study was switched into tsA – 201 cells, as it is challenging to discriminate between  $Ca_v1.2$  and  $Ca_v1.3$ , the two LTCC subtypes expressed in neurons (Zamponi et al., 2015). This is because neurons have long processes (axons and dendrites) which make the resolution of voltage clamp poor, and although  $Ca_v1.2$  and  $Ca_v1.3$  have distinct current, voltage relationships they do overlap.

### 3.1.2 Kinetics of $Ca_v1.2$ and $Ca_v1.3$

At depolarised membrane potentials LTCC's are constantly cycling between closed, open, and inactivated states, as shown in figure 3.1.1 (Hering et al., 2000).

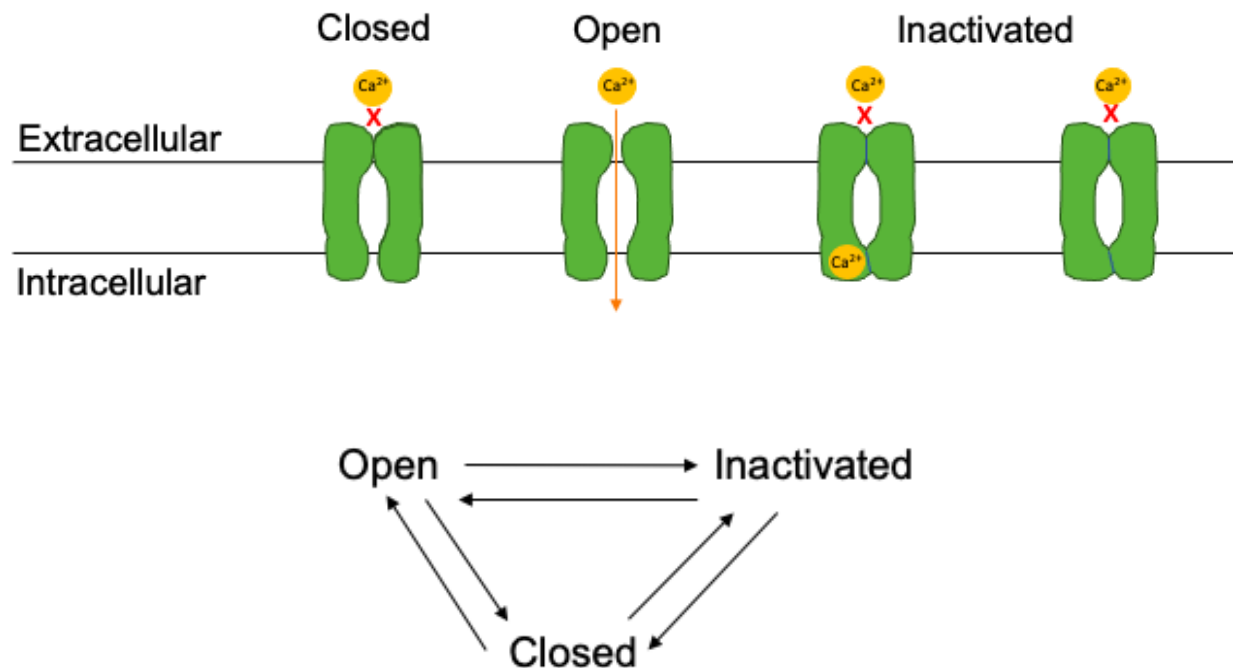


**Figure 3.1.1 LTCC state transitions (information from Hering et al., 2000).** At rest, the majority of the calcium channel population resides in a closed state, where there can be no passage of calcium ions. When the membrane is depolarised, this causes a conformational change which results in the channel being in an open/activated conformation, where there can be entry of calcium ions into the cell. After opening, the channels often move into an inactivated state, which can be calcium (CDI) or voltage dependent (VDI), before transitioning back into a closed state. Although this is the most common series of transitions, channels can move between any state.

When in the open state, the calcium channel is highly selective for calcium ions, despite other cations being at a much higher extracellular concentration (Tang et al., 2014). Evidence suggests that this occurs due to a binding site with a very high affinity for calcium that is formed by the S5/S6 domains of the 4 repeats that compose the pore forming domain (Zamponi, 2005). This site is widely believed to be an EEEE locus, as calcium binding in the pore is abolished by quadruple aspartate, alanine, or glutamine mutations (Cibulsky and Sather, 2000). It is thought that this site is occupied by one or more calcium ions at a time, and the ions permeate the channel due to electrostatic repulsion between different calcium ions (Hess and Tsien, 1984). Simultaneously, this mechanism also prevents the permeation of the channels by any other ions, as the opening of the pore is occluded with calcium ions. A more recent model suggests this process may be more complex, with three calcium binding sites being present within the pore (Tang et al., 2014).

Inactivation of calcium channels is crucial to prevent prolonged depolarisation in brain/heart tissue and toxic calcium overload (Simms and Zamponi, 2014). CDI is thought to be dependent on the binding of calmodulin (CaM), and the mechanism appears conserved between LTCC's. CaM associates with the LTCC  $\alpha$  subunit via its C-terminus binding to the IQ domain (figure 1.2), and an upstream EF-hand region binding to the N-terminus of the  $\alpha$  subunit (Johny et al., 2013). When intracellular calcium rises, the binding of calcium to CaM triggers a conformational change in the channel that leads to CDI. Site directed mutagenesis suggests that this may be due to specific conserved residues within selectivity filter DII (+1) such

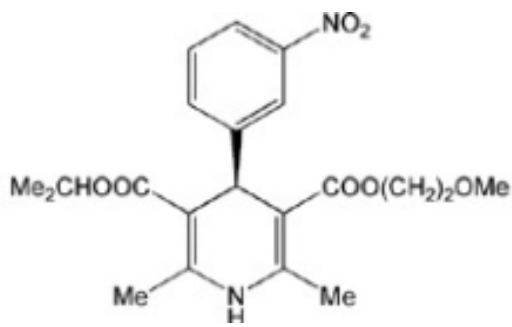
as D707 obscuring the pore when a conformational change is initiated (Abderemane et al., 2019).

In contrast, less is known about the mechanisms of voltage – dependent inactivation. This mechanism is not conserved between calcium channels and so kinetics can differ between LTCC's subtypes (Zhang et al., 1994). It is thought that the residues that may be responsible for this difference are localised in S6 of the first repeat of the  $\alpha$  subunit. Additionally, the identity of the  $\beta$  subunit can also affect inactivation, with  $\beta_3$  promoting VDI and  $\beta_{2a}$  promoting CDI (Findeisen and Minor, 2009)

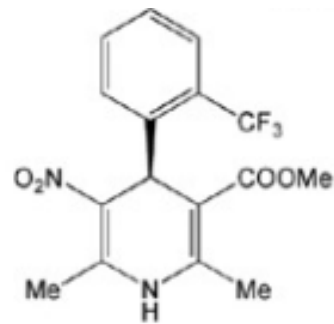
### **3.2.3 Pharmacology of $Ca_v1.2$ and $Ca_v1.3$**

LTCC's are sensitive to block by three main classes of drugs: DHPs, phenylalanine's and benzothiazepines, a feature which is not shared with other types of VGCC's (Striessnig, Ortner and Pinggera, 2015). Block of LTCC's is a well-established treatment for hypertension and cardiac ischemia but is not utilised in the treatment of brain disorders to date. Of the three drug classes, DHP's are the only class which contains agonists as well as antagonists (Tikhonov and Zhorov, 2009). DHP's consist of a six membered ring, with an aromatic moiety and a NH group, as shown in figure 3.1.2. DHP's are thought to primarily bind to and stabilise the LTCC's in their inactivated state, slowing the rate at which channels recover from inactivation and decreasing calcium influx (Striessnig, Ortner and Pinggera, 2015). It has been proposed that when bound to the calcium channel they stabilise a conformation where a single ion is occupying the selectivity filter, and therefore the channel is non-conducting (Peterson and Catterall, 2006).





**Nimodipine**



**Bay K 8644**

**Figure 3.1.2: Structure of a DHP agonist and antagonist a) Nimodipine is a DHP antagonist b) Bay K 8644 is a DHP agonist**

It is known that the DHP binding site is accessed from the extracellular side of the channel and is inside the  $\alpha_1$  pore forming subunit (Kass and Arena, 1989; Kwan et al., 1995). More specifically, studies using site-specific mutations have revealed that the binding site is at the interface between repeats III and IV of the  $\alpha_1$  subunit, and key residues are likely to reside within transmembrane segments IIIS5, IIIS6 and IVS6, as illustrated in figure 3.1.3. (Tikhonov and Zhorov, 2009).

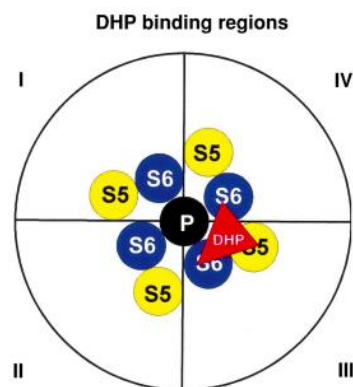


**Figure 3.1.3 : DHP binding regions on the  $\alpha_1$  pore forming subunit of LTCC's.**

## 3.2 Results

### 3.2.1 Untransfected tSA-201 Cells are Devoid of Voltage – Gated Calcium Currents

To establish whether tSA-201 cells have any endogenous currents that may mask a  $\text{Ca}^{2+}$  current, a voltage step from  $-80\text{mV}$  holding potential to  $+20\text{mV}$  was carried out on untransfected cells. This was compared with the current produced from voltage steps in cells expressing exogenous  $\text{Ca}_v1.2$ ,  $\beta_3$ ,  $\alpha_2\delta_1$  (and eGFP). As shown in figure 3.2.1, cells not transfected with  $\text{Ca}_v1.2$  had no visible current, meaning there is no endogenous LTCC expressed. In contrast, those expressing  $\text{Ca}_v1.2$  displayed a current of approximately  $7\text{pA/pF}$ . Cells that were transfected were identified by transfecting eGFP as a marker. The fluorophore was excited by light of wavelength  $488\text{-}509\text{nm}$ . Cells were visualised using a light microscope at  $32\times$  magnification.

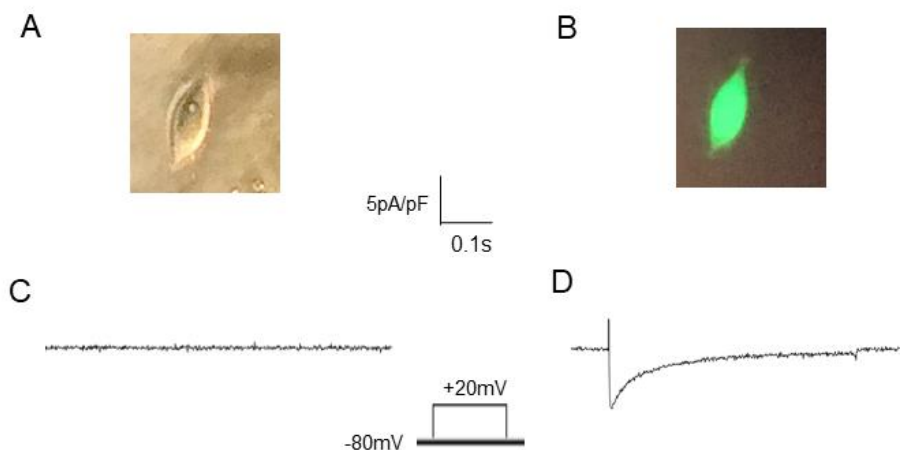


**Figure 3.2.1: tsA-201 cells are devoid of endogenous calcium current** **A)** a transfected cell without exciting eGFP **B)** The same transfected cell when eGFP is excited **C)** Voltage step from a holding potential of  $-80\text{mV}$  to  $+20\text{mV}$  in a cell identified as untransfected **D)** A voltage step from a holding potential of  $-80\text{mV}$  to  $+20\text{mV}$  in a cell identified as transfected

### 3.2.2 Cav1.2 and Cav1.3 Display Distinct Current – Voltage Relationships

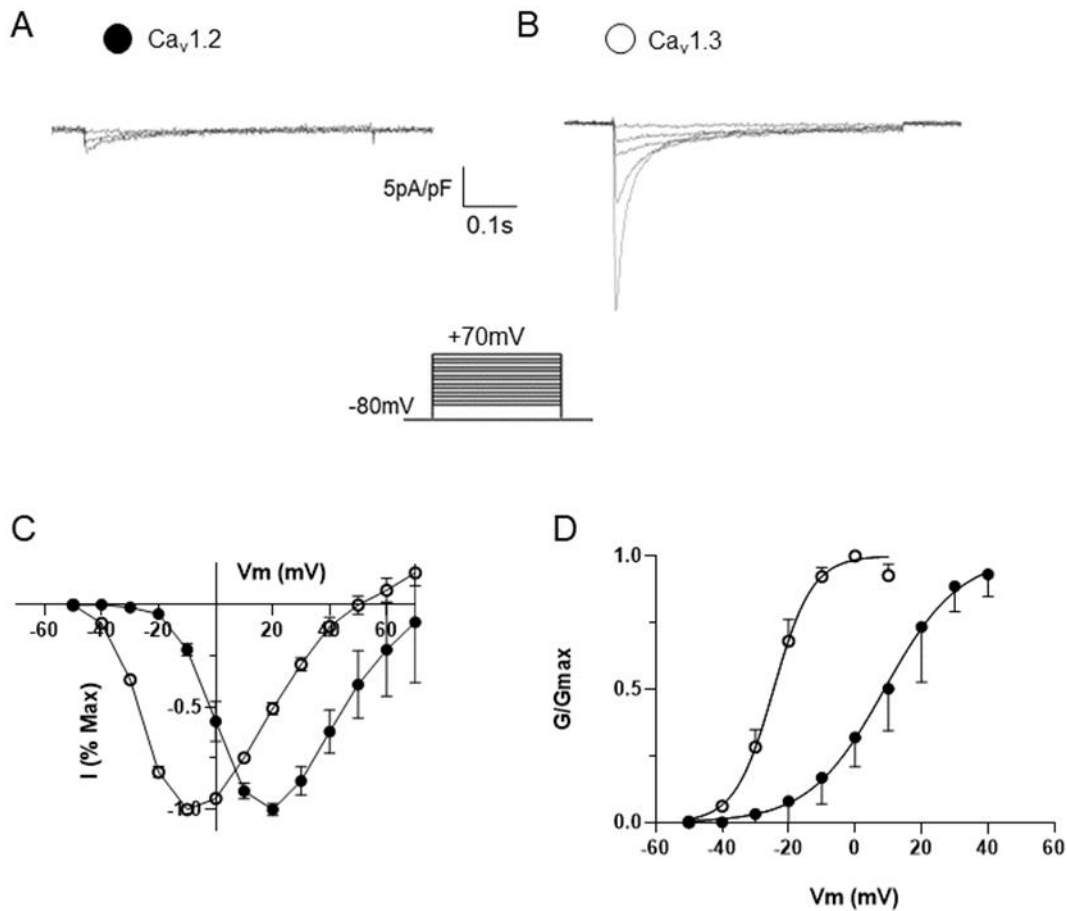


**Figure 3.2.2: Expressed Cav1.2 and Cav1.3 have distinct current-voltage relationships in tsA-201 cells:** Example current traces showing **A)** Cav1.2 transfected cell **B)** Cav1.3 transfected cell **C)** Cav1.2 (●) (n=8) and Cav1.3 (○) (n=8) current voltage relationships normalised to max current **D)** Cav1.2 (●) (n=8) and Cav1.3 (○) (n=8) activation curves generated from peak current.

The electrophysiological characteristics of Cav1.2 were assessed in comparison with Cav1.3, the other LTCC channel expressed in the brain. Both  $\alpha_1$  subunits were expressed with  $\beta_3$  and  $\alpha_2\delta_1$  as auxillary subunits, and eGFP as a marker for

transfection. Cells were incubated overnight in a 37°C incubator before plating ready for patch-clamp experiments approximately 18 hours later.

A current-voltage relationship was produced using voltage steps from a holding potential of -80mV, starting at -50mV and stepping to +70mV in 10mV voltage steps. As shown in figure 3.2.2, the macroscopic current produced by  $Ca_v1.2$  current is high voltage activated in contrast to macroscopic current produced by  $Ca_v1.3$ .  $Ca_v1.2$  produced macroscopic currents that began between -30mV and -20mV and peaked at 20mV. In contrast,  $Ca_v1.3$  macroscopic currents began at -50mV and peaked at -20mV. Cells expressing  $Ca_v1.3$  had an average  $V_{1/2}$  of  $-24.4 \pm 0.64$ mV and slope of  $5.69 \pm 0.111$ . Cells expressing  $Ca_v1.2$  had an average  $V_{1/2}$  of  $14.3 \pm 0.69$ mV and slope of  $7.77 \pm 2.42$ . Unpaired t-tests indicate there is a significant difference between the  $V_{1/2}$  of currents produced by  $Ca_v1.3$  and  $Ca_v1.2$  ( $P < 0.0001$ ), but not the slope.

### **3.3.3 Nimodipine substantially blocks $Ca_v1.2$ mediated current at a Concentration of 10 $\mu$ M**

TsA-201 cells were transfected with  $Ca_v1.2$ , 4R0N tau-eGFP,  $\beta_3$ ,  $\alpha_2\delta_1$ . The cells were incubated in the transfection mixture overnight at 37°C before plating ready for patching. Following this, cells were incubated for another 24 hours at 37°C degrees, and finally, a 24-hour low temperature incubation. Current voltage relationships were generated using step depolarisations, from a holding potential of -80mV, starting at -50mV and increasing to +70mV in 10mV steps. When a control current had been generated (using standard external solution – section 2.6) the external solution was exchanged to one containing 10 $\mu$ M nimodipine. Single step depolarisations, from -

80mV to +20mV, were carried out until the decrease in current had stabilised.

Following this a full IV curve was performed, on the same cell, as shown in figure

### 3.2.3

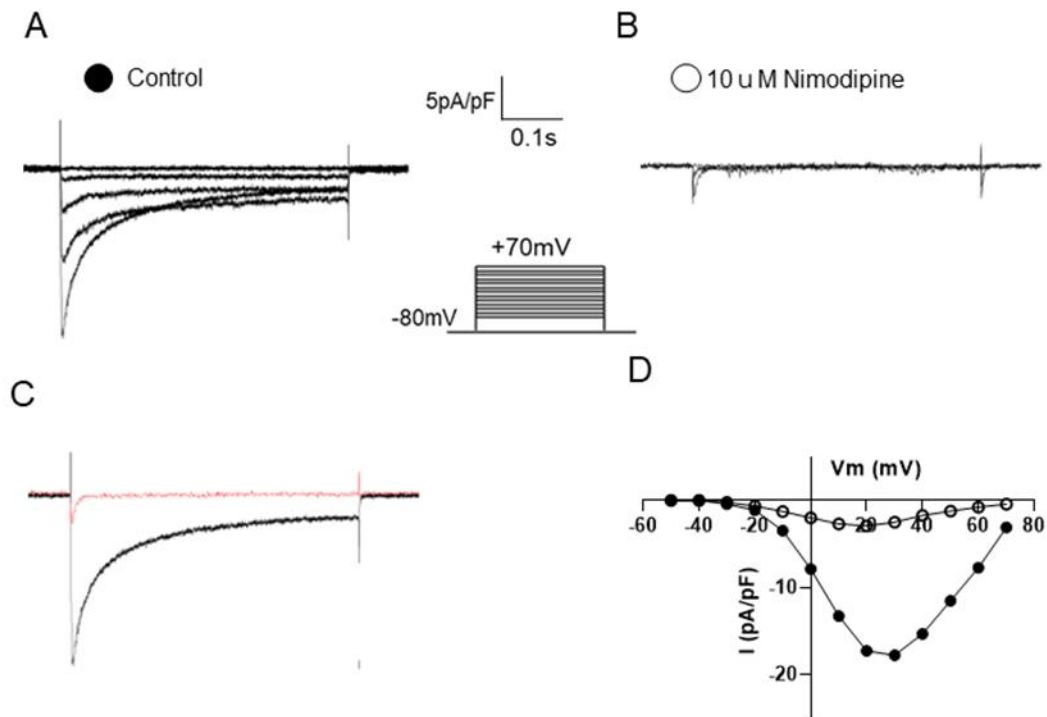


**Figure 3.2.3: Application of 10µM nimodipine markedly decreases Cav1.2 macroscopic current in tsA-201 cells expressing Cav1.2 and 4R0N tau.** Example traces of **A)** Cav1.2 current in the absence of nimodipine **B)** Cav1.2 current in the presence of nimodipine **C)** Superimposed traces of peak current from **A** and **B** **D)** Current voltage relationship for Cav1.2 in the absence (●) (n=2) and presence (○) (n=2) of 10µM nimodipine

In the absence of nimodipine, cells had a mean peak current of -17.7 pA/pF, whereas after application of nimodipine mean peak current was -2.92 pA/pF. This

indicates that with this application of nimodipine approximately 84% of the current is blocked.

### **3.4 Discussion:**

It has been shown that no current is observed in an untransfected tsA-201 cell when it is subject to a voltage protocol that elicits current in  $Ca_v1.2$  transfected cell. This confirms that this cell line is appropriate for the study of expressed  $Ca_v1.2$ , as it is not expressed endogenously. Furthermore, both  $Ca_v1.2$  and  $Ca_v1.3$  mediated currents have similar current voltage relationships to that observed in recent literature (Stan et al., 2022). In both this study and Stan et al., 2022 the peak of  $Ca_v1.2$  mediated current was elicited with a voltage of approximately +20mV, and the peak of  $Ca_v1.3$  mediated current was elicited with a voltage of approximately -10mV. This means that the pore forming and auxiliary subunits are being expressed, as absence of auxiliary subunits would change the kinetics of the channel.

As expected, the  $V_{1/2}$  for  $Ca_v1.2$  and  $Ca_v1.3$  mediated currents was significantly different, and the currents for  $Ca_v1.3$  reach maximum amplitude at relatively hyperpolarised potentials. This is an effect that has been observed in other studies, even though both subtypes are grouped into the HVA class of LTCC's (Xu and Lipscombe, 2001). This confirms that it is possible to easily distinguish between  $Ca_v1.2$  and  $Ca_v1.3$  when expressed in tsA-201 cells. Previous work has shown that this is a property of the  $\alpha_1$  subunit of  $Ca_v1.2/Ca_v1.3$  as it is observed regardless of what auxiliary subunits they are expressed with. In neurones, it is likely that these differences enable for a fine tuning of calcium regulation. There is evidence to

suggest that the subcellular distribution of  $Ca_v1.2$  and  $Ca_v1.3$  in neurones is distinct; with  $Ca_v1.2$  appearing to exist in clusters in the dendrites and soma, and  $Ca_v1.3$  channels being more diffuse (Hell et al., 1993; Bowden et al, 2001). This suggests that the different voltage of activation may enable the channels to carry out different roles, in their specific subcellular locations.

Finally, as expected, application of  $10\mu\text{M}$  nimodipine led to a marked reduction in calcium current. This reduction in peak current demonstrates that  $Ca_v1.2$  channels are being blocked by nimodipine (Tikhonov and Zhorov, 2009). This confirms that the expressed current recorded from the transfected cells can be attributed to LTCC's. In this study the effect of nimodipine on  $Ca_v1.2$  was examined in the presence of 4R0N tau. The effect was comparable to previous studies demonstrating the block of  $Ca_v1.2$  in absence of tau with nimodipine (Xu and Lipscombe, 2001), suggesting that 4R0N tau does not affect the susceptibility of the channel to block by DHP's.  $Ca_v1.3$  current is also blocked by nimodipine, but to a lesser extent (Xu and Lipscombe, 2001).

## **4. Tau Augmentation of LTCC Current**

### **4.1 Introduction**

#### **4.1.1 Increased LTCC Current and Cognitive Decline**

Calcium dysregulation is established to occur with age, and the hypothesis that this leads to cognitive decline has been investigated since the 1980's (Foster and Kumar, 2002). VGCC's are one of the main sources of calcium entry into a cell, and if entry through these channels is not tightly regulated it leads to changes in calcium dependent signalling pathways. As mentioned previously, one of the most notable effects of increased calcium influx via VGCC's is an increase in the amplitude and duration of the AHP, which has a considerable effect on cell excitability (Disterhoft et al., 1996). This can lead to disruption in cognition, which may underlie the memory disturbances we see as people age. Furthermore, augmentation of AHP's leads to alterations in voltage dependent events such as N-methyl-D-aspartate receptor (NMDAR) mediated LTP/ long term depression (LTD) (Foster, 1999). The duration of the calcium transient induced by neuronal stimulation determines whether LTP or LTD occurs from NMDAR activation, with high frequency bursts leading to LTP, and low frequency calcium, over a longer duration, leading to LTD (Bliss et al., 2018). Experiments in aged animals suggests that an increase in LTCC calcium influx will result in an increase in LTD due to an increase in basal calcium levels (Foster and Kumar, 2002). This also results in a decrease in LTP, due to augmented AHP and prolonged refractory period. Exogenous application of calcium onto brain slices from young animals can mimic the age-related imbalance in LTP and LTD, confirming that it is the increase in calcium influx that is responsible for these effects (Norris, Korol



and Foster, 1996). Finally, alterations in calcium homeostasis can increase neurotoxicity, by altering the balance of phosphatases and kinases. Due to the profound effects the above mechanisms have on learning and memory, it is critically important to identify the pathways leading to the increase in calcium influx.

#### **4.1.2 Tau as a Potential Cause of LTCC Current Increase**

Tau is implicated in memory deficits due to its supposed role in AD pathology (Shafiei, Guerrero-Muñoz, Castillo-Carranza, 2017). Despite previous hypotheses focusing on tau tangles, many recent studies support the notion that AD is a disorder of the synapse, and that soluble tau oligomers have a role in this (Jadhav et al., 2015). Transcranial magnetic stimulation (TMS) is a non-invasive technique whereby a magnetic field is applied to the brain and induces depolarisation – thus it can be used to induce LTP/LTD in humans via theta burst stimulation (Koch and Spampinato, 2022). It has been observed that LTD can be consistently induced in patients with AD, however LTP was not observed when submitted to a protocol that induced LTP in healthy age matched controls. What makes these phenomena relevant to the study is that it is possible to speculate that this is occurring due to an increase in calcium current, and that this increase in calcium current is caused by tau. It has been observed that soluble tau is able to induce synaptic dysfunction, and tau cerebrospinal fluid (CSF) levels are associated with a worse disease course (Koch and Spampinato 2022; Koch et al., 2012). In fact, high levels of tau in the CSF of AD patients is associated with an increase in LTD mechanisms and more rapid disease progression. Taken together, this suggests that there is a link between tau overexpression and dysregulation of LTP and LTD. Since increased calcium is also

observed in the aged brain, it is plausible that there are links between these mechanisms.

## 4.2 Results

### 4.2.1 Co-expression of 4R0N Tau with $\text{Ca}_v1.2$ ( $\beta_3$ , $\alpha_2\delta_1$ ) Causes a Significant Increase in Calcium Current Amplitude

tsA-201 cells were transfected with  $\text{Ca}_v1.2\alpha_1$ ,  $\alpha_2\delta_1$  and  $\beta_3$ .  $\text{Ca}_v1.2$  was chosen because  $\text{Ca}_v1.2$  and  $\text{Ca}_v1.3$  are the neuronal LTCC's, with previous work demonstrating that 4R0N tau does not augment  $\text{Ca}_v1.3$  current significantly (Stan et al., 2022). Similarly, 4R0N tau has a  $\text{Ca}_v\beta$  subunit specificity, only augmenting  $\text{Ca}_v1.2$  current when co-expressed with  $\beta_3$ . A control group containing no tau was co-transfected with eGFP as a marker for transfection. In the experimental group, this was co-expressed with 4R0N tau – eGFP (WT 4R0N tau) on a bicistronic vector. 4R0N tau is the isoform of choice for this study because it is the most abundant isoform in the AD brain and has been established to be the only 4R isoform able to significantly increase calcium current (Yasojima, McGeer and McGeer, 1999; Kimur et al, 2016).

The day following transfection cells were seeded into dishes ready for electrophysiological studies and left in a 37°C incubator for approximately 24 hours. The optimisation of the transfection method led to the addition of a 24-hour 27°C incubation following this. Current-voltage relationships for  $\text{Ca}_v1.2$  in the absence and presence of tau were collected with (figure 4.2.2) and without (figure 4.2.1) the low temperature incubation step. Macroscopic current was recorded using a voltage step

protocol, with a holding potential of -80mV. Voltage steps began at -50mV and increased to +70mV in 10 mV voltage steps. Activation curves were plotted using peak current. All experiments were matched and blinded and data for each group collected from three transfections.

As shown in figure 4.2.1 co-expression of 4R0N tau causes an augmentation of  $Ca_v1.2$  macroscopic current, when exogenously expressed in tsA-201 cells. Cells expressing 4R0N tau have a mean peak current of approximately 2x that of control cells ( $-3.11 \pm 0.75$  pA/pF instead of  $-1.50 \pm 0.33$  pA/pF). When compared by a two-way ANOVA the overall effect of expressing 4R0N tau is significant ( $p < 0.0001$ ), with specific points in the voltage curve having a statistically significant difference when compared with multiple comparisons (figure 4.2.1).

Although it increases macroscopic current 4R0N tau does not change the voltage of activation of  $Ca_v1.2$ , as shown by figure 4.2.1 (D). Control cells have a  $V_{1/2}$  of  $9.8 \pm 0.67$ mV and a slope of  $7.8 \pm 2.4$ ; cells co-expressing WT tau have a  $V_{1/2}$  of  $9.9 \pm 0.73$ mV and a slope of  $11.9 \pm 1.6$ . There is no significant difference at any point when an unpaired t-test is used to compare the  $V_{1/2}$  and slope for each point on the voltage curve ( $p > 0.05$ ).

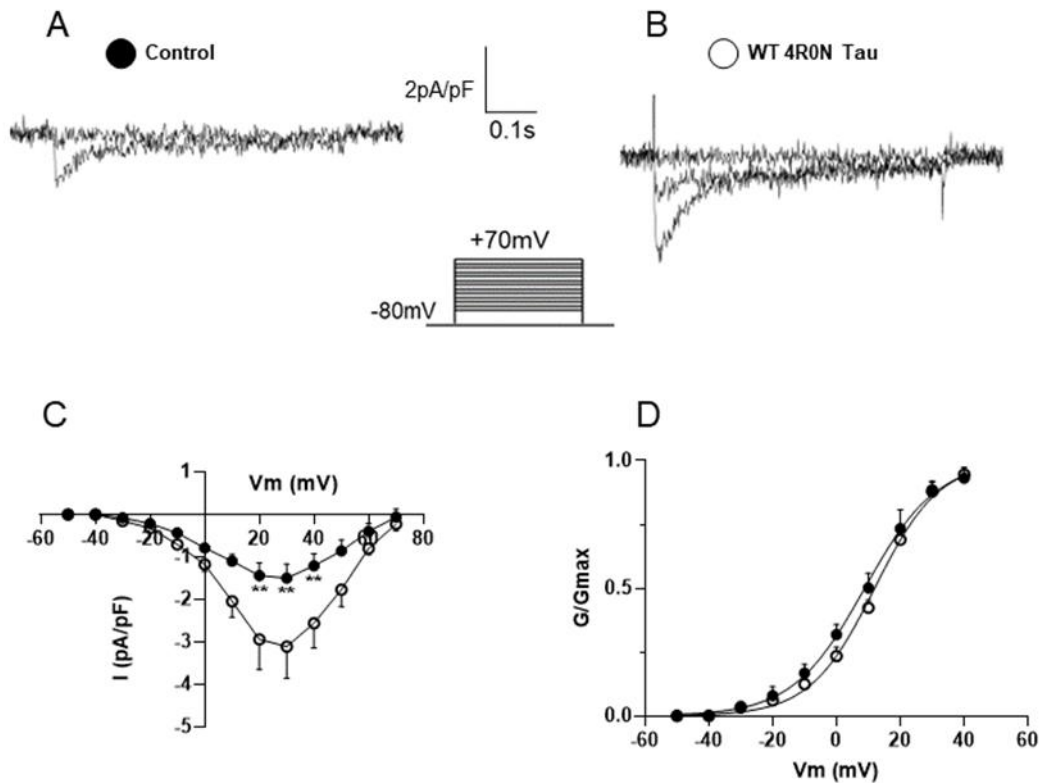


**Figure 4.2.1: Co-expression of 4R0N tau in tsA-201 cells results in augmentation of macroscopic  $Ca_v1.2$  current, without changing activation kinetics.** Representative traces showing **A)**  $Ca_v1.2$  peak current **B)**  $Ca_v1.2$  current in the presence of 4R0N tau **C)** Current – Voltage relationship for  $Ca_v1.2$  in the absence (●) (n=8) and presence of WT 4R0N tau (○) (n=8), \*\* p<0.01 **D)** Activation curve for control (●) (n=8) and WT 4R0N tau (○) (n=8) groups, calculated from peak current shows no significant difference between the groups. Error bars in all figures show SEM

Figure 4.2.2 shows the augmentation of  $Ca_v1.2$  current by 4R0N tau using the adapted transfection method that includes a 24 hour low temperature incubation step (as described in section 2.3.5). This step enabled an additional analysis of the effect

of 4R0N tau on current decay to be performed, as the larger current sizes allowed for greater resolution of currents.

As shown in figure 4.2.2, co-expression of 4R0N tau increases macroscopic exogenous 4R0N tau current. With these transfection conditions cells expressing 4R0N tau have a mean peak current approximately 2.5x larger than control cells ( $-21.83 \pm 4.3$  pA/pF instead of  $-8.22 \pm 1.46$  pA/pF). Two-way ANOVA shows an overall significant effect between groups ( $p < 0.0001$ ) and multiple comparisons revealed the specific voltages at which the difference in current is statistically significant, as shown on figure 4.2.2.

Again, as shown in figure 4.2.2 (D) there is no significant difference between the voltage of activation of  $Ca_v1.2$  mediated current when 4R0N tau is co-expressed. The control group had an average  $V_{1/2}$  of  $8.32 \pm 0.33$  mV and an average slope of  $9.90 \pm 1.12$ . WT 4R0N tau group had an average  $V_{1/2}$  of  $7.78 \pm 0.276$  mV and an average slope of  $5.704 \pm 1.66$ . Unpaired t-test shows no significant differences when  $V_{1/2}$  and slope.

Finally, there appears to be no difference between the current decay of  $Ca_v1.2$  in the presence or absence of 4R0N tau, as shown in figure 4.2.2. The decay was plotted for the data points at the peak of the current. There is no significant difference between decay at any voltage when compared with two-way ANOVA ( $P > 0.05$  for each).

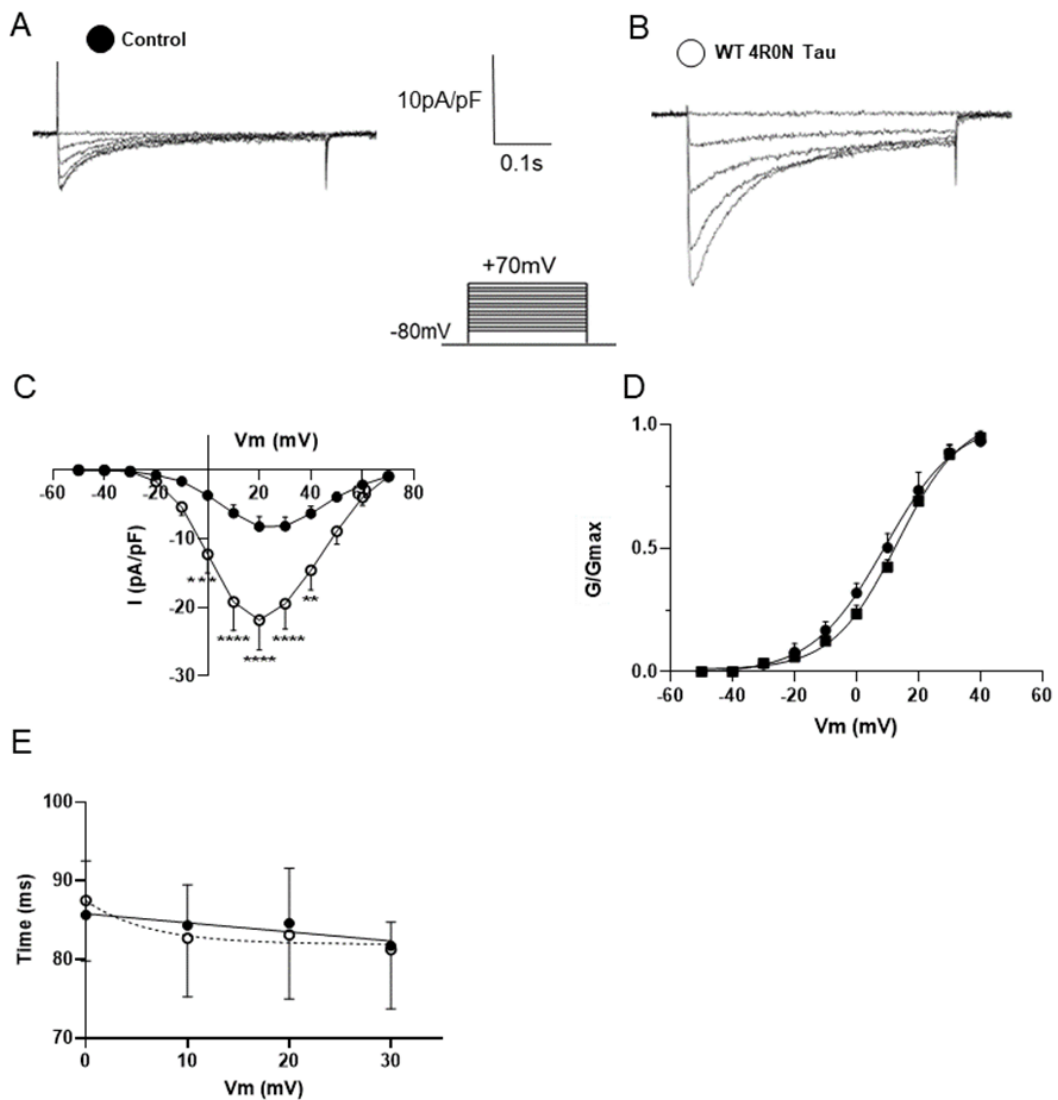


**Figure 4.2.2: Co-expression of 4R0N tau with  $Ca_v1.2$  in tsA-201 cells causes an increase in macroscopic current, without changing channel kinetics.** Data collected from cells incubated at 27°C for 24 hours before recording. Representative traces showing **A)**  $Ca_v1.2$  current **B)**  $Ca_v1.2$  current in the presence of 4R0N tau **C)** Current – Voltage relationship for  $Ca_v1.2$  in the absence (●) (n=12) and presence of WT 4R0N tau (○) (n=12) \*\* p<0.01, \*\*\* p<0.001, \*\*\*\* p<0.0001 **D)** Activation curve for control (●) (n=12) and WT 4R0N tau (○) (n=12) groups, calculated from peak current **E)** Plot to show rate of decay of current at a range of voltage steps in the absence (●) (n=12) and presence (○) (n=12) of 4R0N tau. Error bars in all figures show SEM.

### 4.3 Discussion

This work has substantiated previous findings that expression of 4R0N tau is able to augment macroscopic  $\text{Ca}_v1.2$  mediated current in tsA-201 cells (Stan et al., 2022). This is of interest since it was observed in neurones that overexpression of 4R0N tau caused an increase in the medium and slow AHP, which are thought to be potassium currents that have calcium dependent components (Lima & Marrion, 2007; Stan et al., 2022). In tsA-201 cells, non-stationary noise analysis has indicated that this increase in macroscopic calcium current is occurring due to an increase in calcium channels at the cell membrane (Stan et al., 2022). Here it has been shown that 4R0N tau has no effect on the voltage of activation of  $\text{Ca}_v1.2$  mediated current, or the decay of the  $\text{Ca}_v1.2$  current. This corroborates the finding that tau is increasing calcium channel number, as it further indicates that any increase in calcium current is solely due to an increase in channels at the cell surface membrane, and not changes in the kinetics of individual channels.

It is known that co-expression of membrane associated proteins can lead to increased macroscopic current, for example Rab interacting molecules interact directly with the C-terminus of  $\text{Ca}_v1.3$  ( $\text{Ca}_v1.3$ ,  $\beta_{2a}$ ,  $\alpha_2\delta_1$ ) and cause current augmentation (Picher et al., 2017). Tau is known to be able to interact and bind to many proteins within the cell membrane (Sallaberry, 2021). Furthermore, 4R0N tau has been shown to co-immunoprecipitate (co-IP) with the  $\beta_3$  subunit of  $\text{Ca}_v1.2$ , significantly more than 4R1N tau, an isoform that does not cause  $\text{Ca}_v1.2$  current augmentation (Stan et al., 2022). Taken together these data strongly suggest that

4R0N tau is stabilising functional channels at the cell membrane, via a direct interaction between 4R0N tau and the  $\beta_3$  subunit, and this results in macroscopic current augmentation. This interaction must be very precise as it has both  $\alpha$  and  $\beta$  subunit specificity, and therefore may involve interactions on both subunits, or depend on the conformational changes which the  $\alpha$  subunit induces on the  $\beta$  subunit.

This mechanism could have significant clinical implications for cognitive decline with ageing and in tauopathies. As mentioned in section 1.3, experiments using aged animals with cognitive deficits have demonstrated that application of nimodipine causes reduction in the AHP and an increase in hippocampal neuronal firing, ameliorating memory deficits (Disterhoft et al., 1996). Additionally, hippocampal neurones isolated from aged animals had an increase in  $\text{Ca}_v1.2$  channels at the cell membrane, an increase in L-type calcium current and an increase in size of AHP (Núñez-Santana, et al., 2014; Disterhoft et al., 1996). Since it is known that the ratio of 4R to 3R isoforms of tau increases with age (Yasojima, McGeer, and McGeer, 1999) and with the knowledge that 4R0N tau can augment AHP's and increase  $\text{Ca}_v1.2$  channel expression, it is very plausible that 4R0N tau overexpression is responsible for the above effects.

Furthermore, 4R0N tau may be implicated in AD pathology. The disease is thought to be sporadic, and the initial trigger for the disease is unknown. If cognitive decline was perceived as a spectrum which began with minor deficits and progressed to AD in certain individuals, then it is possible that the 4R0N tau induced increase in calcium channels at the cell membrane is an initial stage of AD. Evidence to support this includes the findings that an excess of 4R isoforms of tau have been reported in



the CSF of individuals with AD (Portelius et al., 2008), as well as an increase in the number of LTCC's on isolated neurones (Coon et al., 1999). Furthermore, a tau mouse model of AD (3xTg-AD) showed an increase in intracellular calcium within cortical neurones, which was largely reduced by inhibition of calcium channels (Lopez et al., 2008). As calcium channel blockers were able to reduce this influx, it is likely that increased stabilisation of  $Ca_v1.2$  at the cell membrane may be a cause. Clinical studies have indicated that the use of nimodipine for the treatment of AD has had some clinical benefit (Nimmrich and Eckert, 2013). Although this is not as marked as would be expected if the above mechanisms are responsible for AD, it is possible that at the point AD has been identified the cellular dysfunction is too severe to be completely reversed.

## 5. Mutagenesis of Tau

### 5.1 Introduction

#### 5.1.1 Structure of Tau

The structure of tau is rather illusive. In monomers it exists as an intrinsically disordered protein, and little is known about ways in which it can fold (Fichou et al., 2019). When probed by x ray diffraction there is a lack of well-defined secondary structure (Skrabana, Sevcik, and Novak, 2006). However, differences in primary structure between tau isoforms are known to impact their binding properties. For example, the number of N-terminal repeats determines which membrane proteins the isoforms preferentially bind, as this is mediated by clusters of threonine/alanine residues on exons 2/3 (Avila et al., 2016). Despite its inherent lack of structure, it has been suggested that it is possible for tau to undergo a gain of structure. For example, a fluorescence resonance energy transfer (FRET) study revealed that tau was able to fold into a 'paper clip' structure, where the C-terminus is in proximity with the microtubule binding domains and the N-terminus, but the N-terminus and microtubule binding domains are distant from one another (Jeganathan et al., 2006). This structure appears to be short lived, as electron paramagnetic resonance showed it still has significant mobility even in this conformation. It is important to remember that although there is some evidence for tau molecules forming secondary structures the literature is sparse and studies have not been repeated.

Despite tau monomers having a lack of secondary structure, hyper-phosphorylation of monomers can lead to aggregation and formation of oligomers and neurofibrillary tangles - known to be a hallmark of neurodegenerative diseases such as AD and

Pick's disease (Scheres et al., 2020; Fichou et al., 2019). Oligomers, like monomers, are poorly defined in terms of structure but are thought to be toxic, leading to behavioural changes and dysfunction at the synapse (Shafiei, Guerrero-Muñoz, Castillo-Carranza, 2017). In contrast to monomers and oligomers, more is known about the structure of tau when it forms tangles. As shown in figure 5.1.1, brain tissue extracted from individuals with various tauopathies has permitted cryo-EM structures to be resolved of tau in different disease states (Scheres et al., 2020). Remarkably, the folding of the filaments is distinct in each disease state, suggesting that different post translational modifications result in distinct folding profiles. This may be due to mutations in the tau gene itself or within proteins that are responsible for the regulation of post-translational modifications. Regardless, this provides insight into just how diverse the folding of tau could be.

The allusivity of tau molecular structure presents a challenge when identifying a region to mutate. Taking an unconservative approach such as a deletion mutation is the most straightforward way to disrupt the structure of tau to prevent an interaction. However, site – directed mutagenesis enables more confidence that the residues that have been chosen are involved in a direct interaction rather than the mutation has caused a conformation change elsewhere in the protein.

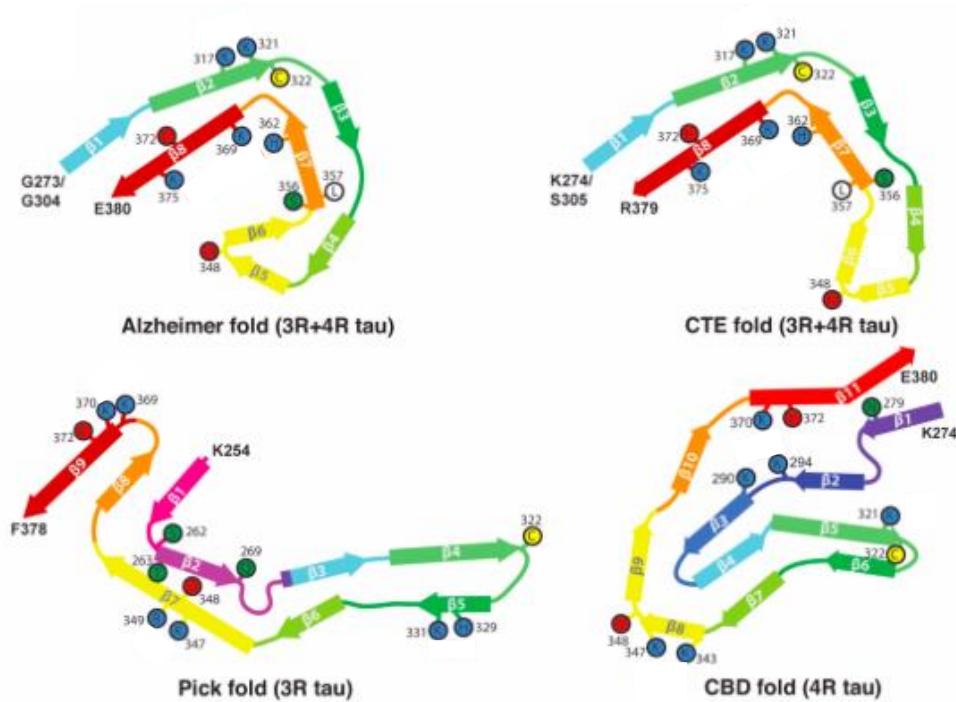


**Figure 5.1.1: Structure of tau filaments in various tauopathies (Scheres et al., 2020).** Models in the XY-Plane. CTE=Chronic Traumatic Encephalopathy CBD = Corticobasal degeneration. Coloured circles denote the position of various amino acid residues.

### 5.1.2 The <sup>166</sup>KKVAVVR<sup>172</sup> region of tau: Influences on structure

The region <sup>224</sup>KKVAVVR<sup>230</sup> (4R2N tau) has been established to be important for the binding of tau to microtubules, alongside the R domains (Li et al., 2020). This sequence is found within the second proline rich domain of tau, as shown in figure 5.1.2. In one study, the importance of the <sup>224</sup>KKVAVVR<sup>230</sup> region was determined by site directed mutagenesis using the ‘looping out’ process to eliminate the desired residues (Goode et al., 1997). The presence of the region <sup>224</sup>KKVAVVR<sup>230</sup> appeared to enhance tau binding to microtubule 3 to 5-fold (Goode et al., 1997). This occurs only in the context of a tau molecule that involves the repeat domains, suggesting

that this effect may be due to an interaction between the two regions, i.e., these residues are responsible for causing tau to fold in such a way that the repeat regions can bind microtubules with a high affinity.

The residues in question were mapped onto 4R0N tau using BLAST, as shown in figure 5.1.3. Residues KKVAVVR were then deleted from 4R0N tau, as described in section 2.5

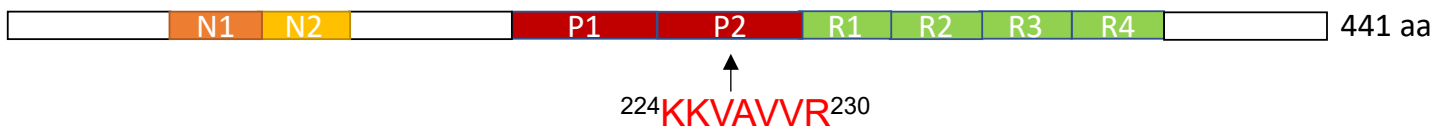


**Figure 5.1.2: Structure of 4R2N tau:** The second proline rich domain consists of residues 166 to 244. KKVAVVR is present in the second proline rich domain (adapted from Fichou et al., 2019)

4R2N Tau: 441aa

<sup>10</sup>  
MAEPRQEFEV MEDHAGTYGL GDRKDQGGYT MHQDQEGDTD AGLKESPLQT  
PTEDGSEEPG SETSDAKSTP TAEDVTAPLV DEGAPGKQAA AQPHTEIPEG TTAEEAGIGD  
TPSLEDEAAG HVTQARMVSK SKDGTGSDDK KAKGADGKTK IATPRGAAPP GQKGQANATR  
IPAKTPPAPK TPPSSGEPK SGDRSGYSSP GSPGTPGSRs RTPSLPTPPT REP<sup>224</sup><sup>230</sup>KKVAVVR  
TPPKSPSSAK SRLQTAPVPM PDLKNVSKI GSTENLKHQP GGGKVQIINK KLDLSNVQSK  
CGSKDNIKHV PGGGSVQIVY KPVDLSKVTS KCGSLGNIHH KPGGGQVEVK SEKLDKDRV  
QSKIGSLDNI THVPGGGNKK IETHKLFRE NAKAKTDHGA EIVYKSPVVS GDTSPRHLSN  
VSSTGSIDMV DSPQLATLAD EVSASLAKQG L

4R0N Tau: 383aa

<sup>10</sup>  
MAEPRQEFEV MEDHAGTYGL GDRKDQGGYT MHQDQEGDTD AGLKAEEAGI  
GDTPSLEDEA AGHVTQARMV SKSKDGTGSD DKKAKGADGK TKIATPRGAA PPGQKGQANA  
TRIPAKTPPA PKTPSSGEP PKSGDRSGYS SPGSPGTPGS RSRTPSLPTP PTREP<sup>166</sup>KKVAV  
<sup>172</sup>VRTPPKSPSS AKSRLQTAPV PMPDLKNVKS KIGSTENLKH QPGGGKVQII NKKLDLSNVQ  
SKCGSKDNIK HVPGGGSVQI VYKPVDLSKV TSKCGSLGNI HHKPGGGQVE VKSEKLDKDRV  
RVQSKIGSLD NITHVPGGGN KKIETHKLF RENAKAKTDH GAEIVYKSPV VSGDTSPRHL  
SNVSSTGSID MVDSPQLATL ADEVASLAK QGL

**Figure 5.1.3: Amino acid sequences of 4R2N and 4R0N tau for deletion mutation.** Highlighted region is region of interest for the deletion mutation. Text in red shows N – terminal domains which are not present in 4R0N tau. This is a 58 amino acid difference.

### **5.1.3 Tau's Proline Rich Domains: Influences on structure and binding**

Since the 1990's, it has been known that proline rich domains are involved in a variety of events inside cells such as cytoskeletal dynamics, trafficking and signal transduction (Musacchio, 2002). Proline residues are also known to influence the structure of proteins (Gerstein, Lesk and Chothia, 1994; Woolfson and Williams, 1990). It is known than proteins preferentially form alpha helices when they have a secondary structure, and the presence of proline residues can change the constraints on this structure, creating a hinge which allows movement, or a kink within the protein. Prolines are known as imino acids, which do not have an amide proton unless positioned at the N-terminus of a protein, and therefore cannot engage in hydrogen bonding (Woolfson and Williams, 1990). Subsequently, proteins that have prolines in internal positions have kinks, which change the folding and flexibility of the protein (von Heijne, 1991).

Proline rich motifs within proteins are also known to be important for mediating protein – protein interactions (Kay, Williamson and Sudol, 2000). Proline rich motifs have certain domains which they bind with a particularly high affinity, such as SH2/3 domains. SH3 domains are approximately 60 amino acids long and are thought to be important in protein – protein interactions which regulate dynamic processes such as internalisation of membrane receptors and transduction of extracellular signals (Musacchio, 2002). SH3 domains are thought to have two hydrophobic binding pockets with a particularly high affinity for PxxP motifs (Kay, Williamson and Sudol, 2000).

### 5.1.4 SH3 Domain of $\text{Ca}_v\beta_3$ : Potential Interactions between 4R0N tau and $\text{Ca}_v\beta_3$ via PXXP Motifs

As discussed in section 1.2,  $\text{Ca}_v\beta_3$  protein contains an SH3 domain, which is conserved between isoforms (Campiglio and Flucher, 2015). However, it is joined to the GK domain by a non-conserved HOOK region, as shown in figure 5.1.4 (Buraei and Yang, 2010). SH3 domains consist of 5 sequential  $\beta$ -strands which are folded into 2 sheets (Larson and Davidson, 2000). The HOOK region links these two sheets together. Like other SH3 domains, they generally bind target proteins via PxxP motifs. However, when visualised in crystal structures, the hydrophobic binding site is partially occluded – thus movement of the HOOK is necessary for binding (Buraei and Yang, 2010). A large section of HOOK is not resolvable as a result of poor electron density, which suggests flexibility in this region. Therefore, it is plausible that such conformational changes occur when binding to the pore forming alpha subunit occurs, or interaction with other proteins.

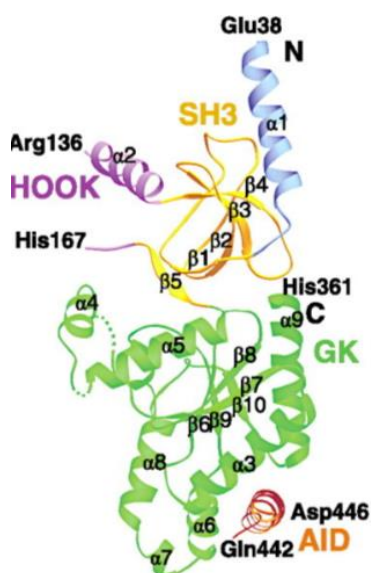


**Figure 5.1.4: Crystal structure of  $\text{Ca}_v\beta_3$  (Buraei and Yang, 2010).** GK = Green, AID = red, HOOK = purple, SH3 = yellow, N-terminus = blue



Tau is known to contain PxxP motifs within its protein rich domain, which are recognised by SH3 domains such as the one on  $Ca_v\beta_3$  (Sallaberry et al., 2021; Avila et al., 2016). In particular, P216 within the P213-P216 motif (numbering based on 4R2N tau) is known to bind SH3 domains with high affinity (Sallaberry et al., 2021). Logically, this presents the possibility that 4R0N tau is augmenting calcium current via an interaction between a PxxP motif, and a hydrophobic binding pocket on the SH3 domain of  $Ca_v\beta_3$ . Co-IP work demonstrated that 4R0N tau can bind  $Ca_v\beta_3$  with a greater potency than 4R1N tau, as illustrated in Figure 5.1.5.

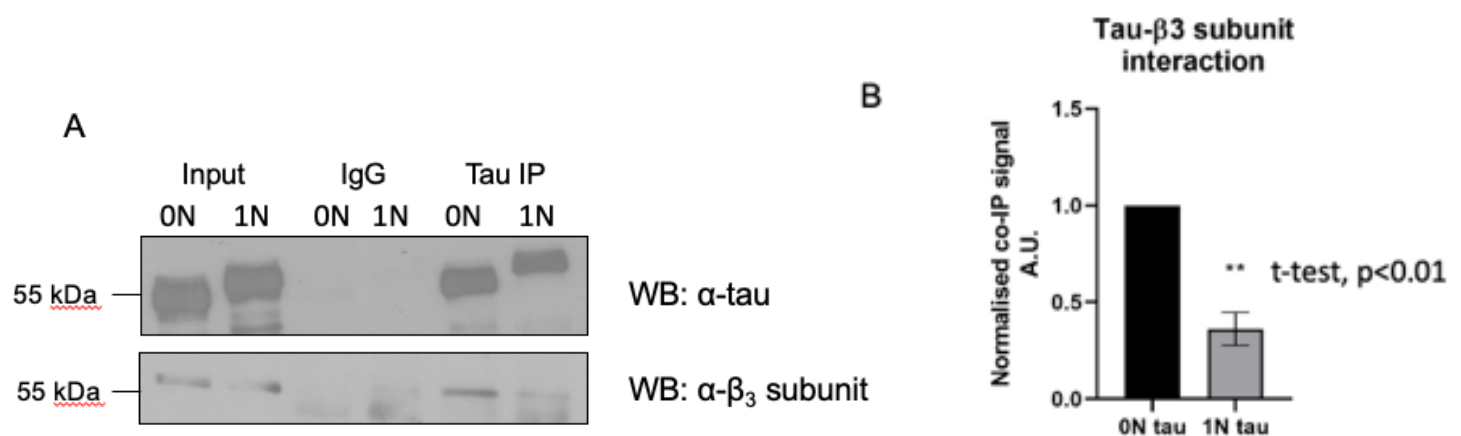


**Figure 5.1.5:  $Ca_v\beta_3$  binds more strongly to 4R0N tau than 4R1N tau in co-IP**

**assays using tau antibody (Stan et al., 2022) A)** Western blot using a  $Ca_v\beta_3$

antibody shows comparable  $Ca_v\beta_3$  expression in cell lysates (input), but a stronger association between 4R0N tau and  $Ca_v\beta_3$  than 4R1N tau. There is comparable tau

input in both groups **B)** When co-IP data are normalised to 4R0N tau label intensity, there is a statistically significantly different difference between the  $\beta_3$  association with 4R0N tau and 4R1N tau.

This result is of importance, firstly because it shows a direct interaction between 4R0N tau and  $Ca_v\beta_3$ . Additionally, since current augmentation is only seen with expression of 4R0N tau, not 4R1N tau, it suggests that this interaction may be related to the effect observed in patch-clamp studies. As from literature the P213-P216 motif is the motif on tau with the highest affinity for SH3 domains (Sallaberry et al., 2021), this was mapped onto 4R0N tau from 4R2N tau as shown in figure 5.1.6, and the residues mutated by substitution to alanine

The prolines of the motif P155 – P158 (4R0N tau) were mutated to alanine's as this is the most common substitution to establish the contribution of a single amino acid to a function (Morrison and Weiss, 2001). This is because alanine's are relatively inert and therefore are less likely to change the conformation or reactivity of the protein – meaning any difference between wild type and mutant is likely due to a loss of the substituted residues, rather than a gain of alanine.

4R2N Tau: 441aa

10  
MAEPRQEFEV MEDHAGTYGL GDRKDQGGYT MHQDQEGDTD AGLKESPLQT  
PTEDGSEEPG SETSDAKSTP TAEDVTAPLV DEGAPGKQAA AQPHTEIEPG  
TTAEEAGIGD TPSLEDEAAG HVTQARMVSK SKDGTGSDDK KAKGADGKTK  
IATPRGAAPP GQKQGQANATR IPAKTTPAPK TPPSSGEPPK SGDRSGYSSP  
213 216  
GSPGTPGSRS RTPSLPTPPT REPKKVAVVR TPPKSPSSAK SRLQTAPVPM  
PDLKNVSKI GSTENLKHQP GGGKVQIINK KLDLSNVQSK CGSKDNIKHV PGGGSVQIVY  
KPVDSLKVTS KCGSLGNIHH KPGGGQVEVK SEKLDKDFKDRV  
QSKIGSLDNI THVPGGGNKK IETHKLTFRE NAKAKTDHGA EIVYKSPVVS GDTSPRHLSN  
VSSTGSIDMV DSPQLATLAD EVSASLAKQG L

4R0N Tau: 383aa

10  
MAEPRQEFEV MEDHAGTYGL GDRKDQGGYT MHQDQEGDTD AGLKAEEAGI  
GDTPSLEDEA AGHVTQARMV SKSKDGTGSD DKKAKGADGK TKIATPRGAA  
PPGQKQGQANA TRIPAKTPPA PKTPPSSGEP PKSGDRSGYS SPGSPGTPGS  
155 158  
RSRTPSLPTP PTREPKKVAV VRTPPKSPSS AKSRLQTAPV PMPDLKNVKS  
KIGSTENLKH QPGGGKVQII NKKLDLSNVQ SKCGSKDNIK HVPGGGSVQI VYKPVDSLKV  
TSKCGSLGNI HHKPGGGQVE VKSEKLDKFD RVQSKIGSLD NITHVPGGGN KKIETHKLTF  
RENAKAKTDH GAEIVYKSPV VSGDTSPRHL SNVSSTGSID MVDSPQLATL  
ADEVSASLAK QGL

**Figure 5.1.6: Amino acid sequences of 4R2N and 4R0N tau for substitution mutation.** Highlighted region is region of interest for mutation. Text in red shows N – terminal domains which are not present in 4R0N tau. This is a 58 amino acid difference.

## 5.2 Results

### 5.2.1 Deletion of region <sup>166</sup>KKVAVVR<sup>172</sup> does not diminish current augmentation

tsA-201 cells were transfected with Cav1.2, Cav $\alpha_2\delta_1$  and Cav $\beta_3$ . For the control group (no tau) this was co-expressed with eGFP; in the experimental groups the channel was co-expressed with WT 4R0N tau-eGFP (WT 4R0N tau), or 4R0N tau with residues 166-172 deleted, on a bicistronic vector with eGFP (<sup>166-172</sup>del4R0N tau). The cells were seeded into dishes approximately 12-24h after transfection and left in a 37°C incubator for another 16-24 hours before patch-clamp studies. Current – voltage relationships for macroscopic calcium current were generated using a voltage step protocol, increasing to +70mV in 10mV steps, starting from -50mV; holding potential prior to voltage steps is -80mV. These data were also used to plot activation curves from peak current. All experiments were matched and blinded, and data for each group collected from three separate transfections.

As shown in figure 5.2.1 <sup>166-172</sup>del4R0N tau appears to augment Cav1.2- mediated current to the same extent as WT 4R0N tau. Mean peak voltage is  $-1.50 \pm 0.33$  pA/pF for control cells,  $-3.11 \pm 0.75$  pA/pF for WT 4R0N tau and  $-3.17 \pm 0.84$  pA/pF for <sup>166-172</sup>del 4R0N tau. Two-way ANOVA with multiple comparisons revealed no statistically significant difference between Cav1.2 current when co-expressed with WT 4R0N tau or <sup>166-172</sup>del4R0N tau ( $p > 0.05$ ). However, when compared to control group, both WT and <sup>166-172</sup>del4R0N tau caused a statistically significant increase in calcium current at peak voltages (figure 5.2.1, figure 4.2.1).

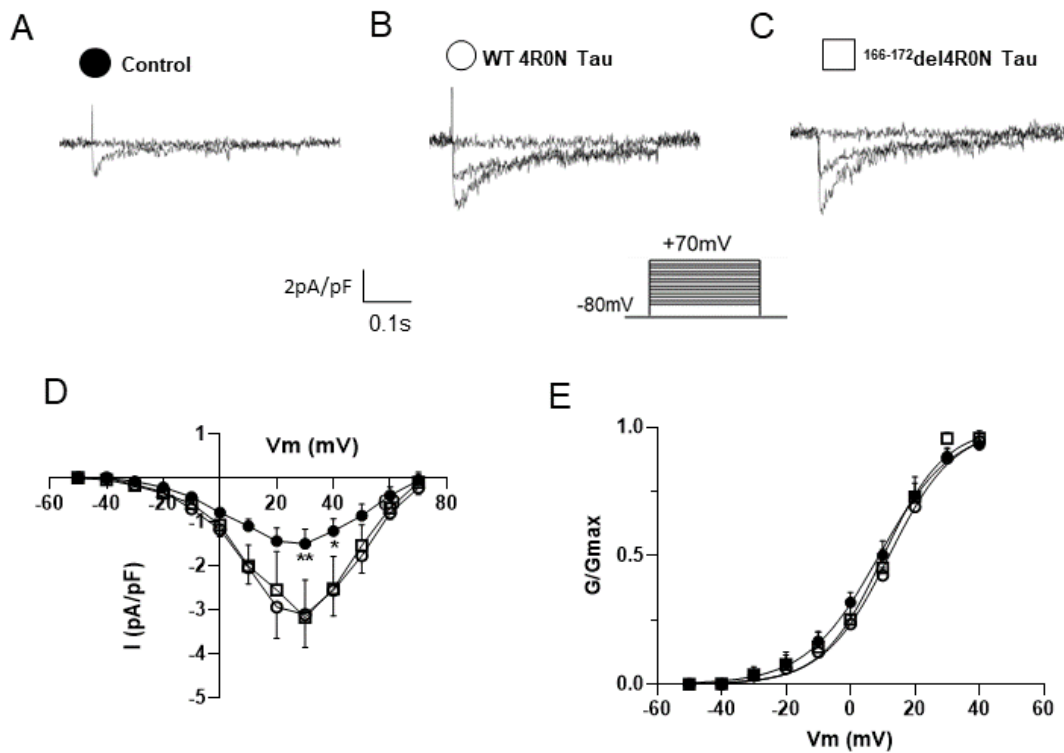


**Figure 5.2.1:**  $^{166-172}\text{del4R0N}$  tau augments macroscopic  $\text{Ca}_v1.2$  current in tsA-201 cells to the same extent as WT 4R0N tau. Representative trace of **A)**  $\text{Ca}_v1.2$  peak current **B)**  $\text{Ca}_v1.2$  current in the presence of WT 4R0N tau **C)**  $\text{Ca}_v1.2$  current in the presence of  $^{166-172}\text{del4R0N}$  tau **D)** Current – voltage relationship for  $\text{Ca}_v1.2$  in the absence ( $\bullet$ ) ( $n=8$ ) and presence of WT 4R0N tau ( $\circ$ ) ( $n=8$ ) or  $^{166-172}\text{del4R0N}$  tau ( $\square$ ) ( $n=7$ ). Points of statistically significant difference in  $\text{Ca}_v1.2$  current when expressed in absence and presence of  $^{166-172}\text{del4R0N}$  tau denoted by \*  $p<0.05$ , \*\*  $p<0.01$  **E)** Activation curve for control ( $\bullet$ ) ( $n=8$ ), WT 4R0N tau ( $\circ$ ) ( $n=8$ ) and  $^{166-172}\text{del4R0N}$  tau ( $\square$ ) ( $n=7$ ) calculated from peak current. Error bars in all figures show SEM.

There was no effect of co-expression of WT 4R0N tau or  $^{166-172}\text{del4R0N}$  tau on the voltage dependence of activation of  $\text{Ca}_v1.2$  channels. Control cells had a  $V_{1/2}$  of  $9.8 \pm 0.67\text{mV}$  and a slope of  $7.8 \pm 2.4$ ; cells co-expressing WT tau had a  $V_{1/2}$  of  $9.9 \pm$

0.73mV and a slope of  $11.9 \pm 1.6$ ; cells co-expressing <sup>166-172</sup>del4R0N tau had a  $V_{1/2}$  of  $8.4 \pm 0.56$ mV and a slope of  $9.6 \pm 3.6$ . One way ANOVA  $p > 0.05$  when comparing  $V_{1/2}$  and slope.

### **5.2.2 P155A/P158A Mutations Abolish Tau's Ability to Augment Current**

tsA-201 cells were transfected with  $Ca_v1.2\alpha_1$ ,  $Ca_v\alpha_2\delta_1$  and  $Ca_v\beta_3$  subunits. In control cells (no tau) these units were co-expressed with eGFP. In the experimental groups, the calcium channel was co - expressed with WT 4R0N tau – eGFP (WT 4R0N tau), or PP155/8AA 4R0N tau – eGFP (PP155/8AA 4R0N tau). Cells were transfected and macroscopic currents recorded as described in 4.2.2. However, an additional 24-hour low temperature incubation step was added between seeding and patch-clamp studies to increase throughput, as described in section 2.3.5.

Mutation of residues P155 and P158 to alanine abolishes the ability of 4R0N tau to augment macroscopic calcium current in tsA-201 cells. Mean peak current for control was  $-8.22 \pm 1.46$ pA/pF, for WT tau  $-21.83 \pm 4.3$ pA/pF, and for mutant tau  $-9.87 \pm 3.47$ pA/pF. Two-way ANOVA with multiple comparisons revealed that when compared with control and PP155/8AA 4R0N tau group, co-expression with WT 4R0N tau caused a statistically significantly augmentation in  $Ca_v1.2$  current at several points of the voltage curve, as shown in figure 5.2.2/4.2.2. There is no statistically significant difference between the current size in control groups or with co-expression of PP155/8AA 4R0N tau at any voltage ( $p > 0.05$ ).

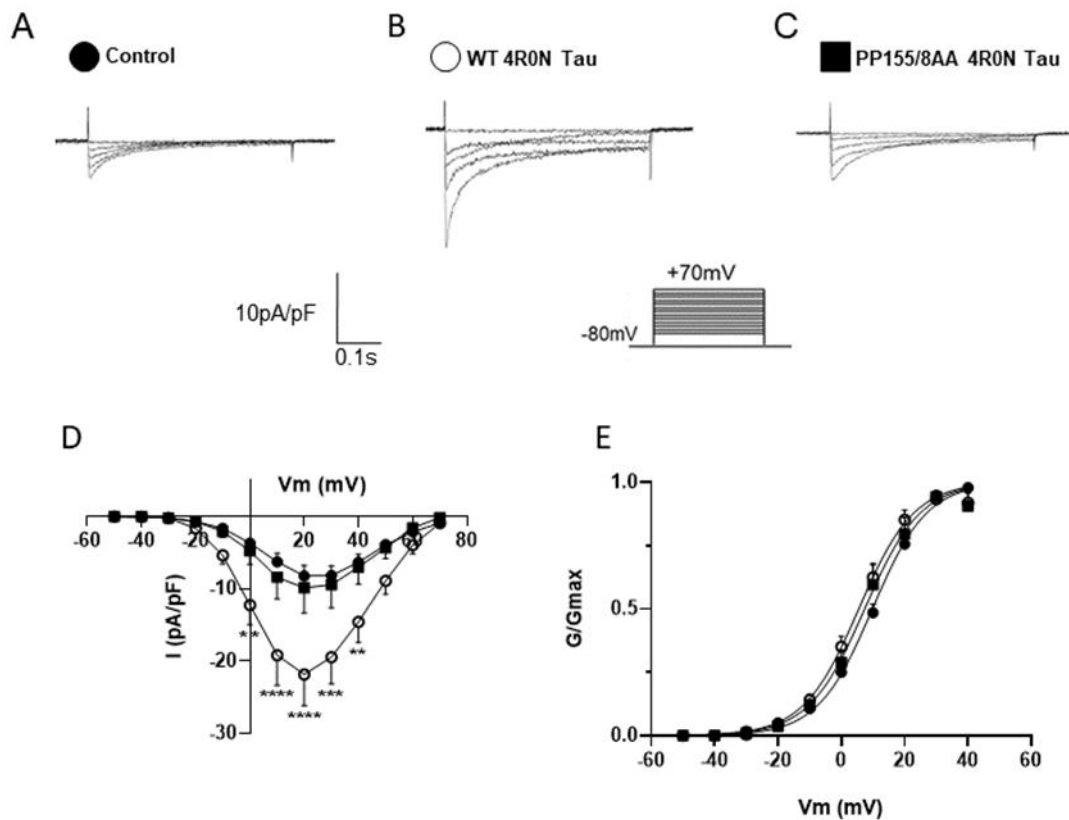


**Figure 5.2.2: Mutation of prolines 155 and 158 to alanine abolishes 4R0N tau augmentation of macroscopic calcium current in tsA-201 cells, without changing activation kinetics.** Representative trace of **A**)  $\text{Ca}_v1.2$  current **B**)  $\text{Ca}_v1.2$  current in the presence of WT 4R0N tau **C**)  $\text{Ca}_v1.2$  current in the presence PP155/8AA 4R0N tau **D**) Current – voltage relationship for  $\text{Ca}_v1.2$  in the absence (●) (n=12) and presence of WT 4R0N tau (○) (n=12) or PP155/8AA 4R0N tau (■) (n=9) Points of statistically significant difference in  $\text{Ca}_v1.2$  current when expressed with either WT 4R0N tau or PP155/8AA 4R0N tau denoted by \*\* p<0.01, \*\*\* p<0.001, \*\*\*\*p<0.0001 **E**) Activation curves for control (●) (n=12), WT 4R0N tau (○) (n=12) and PP155/8AA 4R0N tau (■) (n=9), calculated from peak current. Error bars on all figures show SEM.

As shown in figure 5.2.2 each group had overlapping voltage dependence of activation, suggesting that there is no change in the activation voltage of the channel due to expression of WT or PP155/8AA 4R0N tau. The control group had an average  $V_{1/2}$  of  $8.32 \pm 0.33$ mV and an average slope of  $9.90 \pm 1.12$ . WT 4R0N tau group had an average  $V_{1/2}$  of  $7.78 \pm 0.2$ mV and an average slope of  $5.704 \pm 1.66$ . Finally, P155/158A tau group had a  $V_{1/2}$  of  $7.31 \pm 0.89$ mV and an average slope of  $7.78 \pm 2.36$ . One way ANOVA shows no significant difference when comparing the  $V_{1/2}$  or slope between any of the groups ( $P > 0.05$ ).



### 5.3 Discussion

Here it has been demonstrated that mutation of residues P155 and P158 of 4R0N tau to alanine can abolish the current augmentation that was seen when WT 4R0N tau was co-expressed with Ca<sub>v</sub>1.2 channels in tsA-201 cells. This is a highly significant effect, with Ca<sub>v</sub>1.2 mediated current in the presence of PP155/8AA 4R0N tau being of similar amplitude to control. In contrast, deletion of residues 166-172 does not have any effect on the ability of 4R0N tau to augment current, with Ca<sub>v</sub>1.2 current in the presence of <sup>166-172</sup>del4R0N tau being comparable to co-expression with WT 4R0N tau. In all conditions, there was no significant difference in the V<sub>1/2</sub> of Ca<sub>v</sub>1.2 mediated current demonstrating that co-expression of the WT and mutants of 4R0N tau did not alter activation kinetics of the channel.

It is surprising that there was such a marked difference in the effect of the two mutants, considering the residues are closely located in the second proline rich domain of tau, as shown in figure 5.3.1 (Fichou et al., 2019). Additionally, previous work has suggested that <sup>166-172</sup>del4R0N tau has disrupted folding, which is typically thought to interfere with protein interactions (Good et al., 1997). However, as tau is an intrinsically disordered protein (Fichou et al., 2019), it is possible that it takes up different conformations when it is bound to different proteins. Residues 166-172 may be important for the conformation where it is able to bind microtubules, but not the conformation that tau is in when it binds Ca<sub>v</sub>β<sub>3</sub>. This is different from proteins that have substantial secondary and tertiary structure, where a deletion of a large region is likely to impact its binding to most proteins.



**Figure 5.3.1: Residues P155/P158 and KKVAVVR are both located in the second proline rich domain of 4R0N tau.** Proline residues substituted to alanine (green) and KKVAVVR residues deleted (red)

In support of this idea, there is evidence to suggest that tau is a flexible protein, potentially even taking up different conformations in different situations. It has been shown through cryo-EM studies that when existing as filaments, tau takes up different conformations that are specific to various disease states (figure 5.1.1; Scheres et al., 2020). Although this is not directly translatable to tau monomers, it seems highly likely that they can take up different conformations to create these varied filaments. Additionally, a FRET study has revealed that tau is able fold into a ‘paper-clip’ conformation, but that this is short-lived, and tau retains its mobility (Jeganathan et al., 2006). Although our understanding of the structure of tau monomers is very limited, taken together the evidence suggests that its structural disorder means that it is very mobile and could adopt several different conformations. It is possible that this is an explanation for the distinct effects of <sup>166-172del</sup> 4R0N tau and PP155/8AA 4R0N tau, despite the close proximity of these residues in tau.

If the above is true, then it follows that the residues P155 and P158 are crucial in the binding of tau to  $\text{Ca}_v\beta_3$ . It is possible that this interaction is direct, as the ability of

4R0N tau to augment  $\text{Ca}_v1.2$  current is completely abolished with these mutations, though this cannot be established from electrophysiology alone. It is logical that these residues would be the point of direct interaction between  $\text{Ca}_v1.2$  and 4R0N tau, as PXXP motifs are known to bind  $\text{SH}_3$  domains, which is present on the  $\beta_3$  subunit of  $\text{Ca}_v1.2$  (Sallaberry et al., 2021). Co-IP studies have shown that 4R0N tau is able to bind  $\beta_3$ , whereas 4R1N tau (an isoform that does not cause  $\text{Ca}_v1.2$  current augmentation) does not (Stan et al., 2022). I propose that 4R0N tau directly binds to the  $\beta_3$  subunit of  $\text{Ca}_v1.2$ . This interaction involves residues P155 and P158 of 4R0N tau, and residues within the  $\text{SH}_3$  domain of  $\beta_3$ . It is possible that this interaction enables 4R0N tau to stabilise  $\text{Ca}_v1.2$  at the cell membrane, causing an increase in macroscopic current. Co-IP data showing that PP155/8AA 4R0N tau does not bind  $\beta_3$  will be crucial in providing evidence to support this hypothesis.

A potential drawback of this hypothesis is that the effect of 4R0N tau on  $\text{Ca}_v1.2$  current has a  $\beta$  subunit specificity, only augmenting current when expressed with  $\beta_3$  (Stan et al., 2022). This is confounding because all  $\beta$  subunits have a conserved  $\text{SH}_3$  domain, to which PxxP motifs would be able to bind (Campiglio and Flucher, 2015). However, crystal structures of  $\text{Ca}_v\beta_3$  reveal that the  $\text{SH}_3$  domain is occluded by the non-conserved HOOK region, and movement of this region is necessary for binding (Buraei and Yang, 2010). This region is thought to have flexibility and may move when the  $\beta$  subunit binds other proteins. Therefore, the length and composition of the HOOK region may be a factor in determining whether 4R0N tau can access the  $\text{SH}_3$  domain to bind and would explain the differences observed when tau is expressed with different  $\beta$  subunit isoforms. Although all speculation, it is possible that this mechanism would also provide an explanation for the  $\alpha$  subunit specificity of

the 4R0N tau effect. Since the HOOK region of the  $\beta$  subunit moves to expose the SH<sub>3</sub> domain on binding of the  $\beta$  subunit to other proteins, it is possible that different  $\alpha$  subunits result in different movement of the HOOK domain. The outcome of this is that the access of 4R0N tau to the SH<sub>3</sub> domain, which it would bind via PxxP motifs, changes.

Additional to this work, insight into the mechanisms of the channels underlying the AHP will be essential for furthering knowledge in this field. It has been suggested that small conductance calcium-activated potassium (SK) channels are crucial in generating the sAHP (Sahu and Turner, 2021). As mentioned previously, inhibition of LTCC's in hippocampal slice preparations drastically reduced the  $I_{sAHP}$  and had moderate effects on the  $I_{mAHP}$  (Lima and Marrion, 2007), explaining the link between increase in calcium influx and a decrease in neuronal firing. What is particularly interesting about this phenomenon is that it was shown using cell attached patches in hippocampal neurones that the delay of SK channel opening after LTCC opening suggests that the channels are approximately 50-150nm apart (Marrion and Tavalin, 1998), though it is unknown how these microdomains are created. Although much more work needs to be conducted to investigate this idea, it is an exciting possibility that the protein anchoring LTCC's and channels underlying the  $I_{sAHP}$  together is a filament of tau, since the length of a tau filament is thought to be around 100nm (Ferrari et al., 2003; Necla and Kuret, 2004), which is the hypothesised gap separating an SK and LTCC (Marrion and Tavalin, 1998).

Better understanding of the interaction between 4R0N tau and Ca<sub>v</sub>1.2 could potentially provide insight into the mechanisms underlying cognitive decline with

ageing and in AD. As described in section 4, an increase in  $Ca_v1.2$  expression at the cell membrane, and in 4R0N tau has been observed in both animals and humans that experience cognitive decline (Núñez-Santana, et al., 2014; Portelius et al., 2008; Coon et al., 1999; Thompson, Deyo and Disterhoft, 1990). The evidence presented here demonstrates that tau is inextricably linked to calcium influx through LTCC's and subsequently the AHP. More investigation into the role of tau in regulating the AHP could revolutionise our understanding of neuronal firing, and potentially provide invaluable insights into the processes regulating learning and memory.

## 6. Future Work

As stated in section 5.3, it will be necessary to perform a Co-IP to establish that P155 and P158 mutations prevent the interaction between 4R0N tau and  $\beta_3$ . It will then be important to further understand the  $\beta$  subunit specificity of 4R0N tau augmentation of Cav1.2 current. Substituting the HOOK region from  $\beta_{2a}$  onto  $\beta_3$  would be a useful investigation, as co-expression of 4R0N tau with Cav1.2 and  $\beta_{2a}$  does not result in current augmentation (Stan et al., 2022). In terms of translating the investigation into animal models, it will be necessary to look at the effect of overexpression of 4R0N tau mutants on calcium current in brain slices, and the amplitude of the AHP in hippocampal neurones. Considering the data shown above in tsA-201 cells, it would be expected that expression of PP155/8AA 4R0N tau would not lead to calcium current augmentation and therefore would have no effect on the AHP.

If it can be confirmed that PP155/8AA 4R0N tau does not cause current augmentation in brain slices, then the next stage would be to assess the effect of WT 4R0N tau compared to PP155/88AA 4R0N tau on the ability of animals to perform memory-based tasks. If it is established that WT 4R0N tau overexpression results in memory deficits, whereas over expressing PP155/88AA 4R0N tau does not, then the next phase would be to create a small molecule that disrupts the interaction between WT 4R0N tau a Cav $\beta_3$  to evaluate if this can ameliorates memory deficits in aged animals, and animal models of AD. Alternately, the same outcome could be achieved by creating a small molecule that attenuates the currents that underly the mAHP and

sAHP, as it is the increase in the amplitude of these currents that directly leads to a decrease in neuronal firing.

## 7. Conclusion

Co-expression of 4R0N tau with Cav1.2, Cav $\beta$ <sub>3</sub> and  $\alpha$ <sub>2</sub> $\delta$ <sub>1</sub> results in a significant augmentation of Cav1.2 mediated current. *In vitro* in hippocampal cells this leads to an increase in the AHP. *In vivo* increased LTCC and AHP is known to lead to a decrease in the rate of neuronal firing and this has been correlated with a decrease in cognition. Previous work suggested that 4R0N tau was able to increase Cav1.2 mediated current by a direct interaction with Cav $\beta$ . It is thought that 4R0N tau is stabilising Cav1.2 channels in the membrane as it can increase macroscopic current without altering any individual channel properties. This study has shown that residues P155 and P158 are crucial for the interaction that leads to augmentation of Cav1.2 mediated current by 4R0N tau. When P155 and P158 are mutated to alanine co-expression of 4R0N tau does not cause any change in the amplitude of Cav1.2 mediated current. It is hypothesised that mutation of P155 and P158 disrupts a direct interaction between 4R0N tau and residues within the SH3 domain of Cav $\beta$ <sub>3</sub>.



## Bibliography

- Abderemane-Ali, F., Findeisen, F., Rossen, N.D. and Minor Jr, D.L., 2019. A selectivity filter gate controls voltage-gated calcium channel calcium-dependent inactivation. *Neuron*, 101(6), pp.1134-1149.
- Avila, J., Jiménez, J.S., Sayas, C.L., Bolós, M., Zabala, J.C., Rivas, G. and Hernández, F., 2016. Tau structures. *Frontiers in aging neuroscience*, 8, p.262.
- Bliss, T.V., Collingridge, G.L., Morris, R.G. and Reymann, K.G., 2018. Long-term potentiation in the hippocampus: discovery, mechanisms and function. *Neuroforum*, 24(3), pp.A103-A120.
- Bowden, S.E., Fletcher, S., Loane, D.J. and Marrion, N.V., 2001. Somatic colocalization of rat SK1 and D class (Cav 1.2) L-type calcium channels in rat CA1 hippocampal pyramidal neurons. *Journal of Neuroscience*, 21(20), pp.RC175-RC175.
- Buraei, Z. and Yang, J., 2010. The  $\beta$  subunit of voltage-gated  $\text{Ca}^{2+}$  channels. *Physiological reviews*, 90(4), pp.1461-1506
- Burdyga, T. and Wray, S., 2005. Action potential refractory period in ureter smooth muscle is set by Ca sparks and BK channels. *Nature*, 436(7050), pp.559-562.
- Burke, S.N. and Barnes, C.A., 2006. Neural plasticity in the ageing brain. *Nature reviews neuroscience*, 7(1), pp.30-40.
- Campiglio, M. and Flucher, B.E., 2015. The role of auxiliary subunits for the functional diversity of voltage-gated calcium channels. *Journal of cellular physiology*, 230(9), pp.2019-2031.
- Carbone, E.L.H.D. and Lux, H.D., 1984. A low voltage-activated, fully inactivating Ca channel in vertebrate sensory neurones. *Nature*, 310(5977), pp.501-502.
- Catterall, W.A., 2011. Voltage-gated calcium channels. *Cold Spring Harbor perspectives in biology*, 3(8), p.a003947.
- Cibulsky, S.M. and Sather, W.A., 2000. The EEEE locus is the sole high-affinity  $\text{Ca}^{2+}$  binding structure in the pore of a voltage-gated  $\text{Ca}^{2+}$  channel: block by  $\text{Ca}^{2+}$  entering from the intracellular pore entrance. *The Journal of General Physiology*, 116(3), pp.349-362
- Clozel, J.P., Ertel, E.A. and Ertel, S.I., 1997. Discovery and main pharmacological properties of mibefradil (Ro 40-5967), the first selective T-type calcium channel blocker. *Journal of hypertension*, 15(5), pp.S17-S26.

Coon, A. L., Wallace, D. R., Mactutus, C. F. & Booze, R. M. L-type calcium channels in the hippocampus and cerebellum of Alzheimer's disease brain tissue. *Neurobiol. Aging* 20, 597–603 (1999).

Dalby, B., Cates, S., Harris, A., Ohki, E.C., Tilkins, M.L., Price, P.J. and Ciccarone, V.C., 2004. Advanced transfection with Lipofectamine 2000 reagent: primary neurons, siRNA, and high throughput applications. *Methods*, 33(2), pp.95-103.

Davies, A., Douglas, L., Hendrich, J., Wratten, J., Van Minh, A.T., Foucault, I., Koch, D., Pratt, W.S., Saibil, H.R. and Dolphin, A.C., 2006. The calcium channel  $\alpha 2\delta$ -2 subunit partitions with CaV2. into lipid rafts in cerebellum: implications for localization and function. *Journal of Neuroscience*, 26(34), pp.8748-8757.

Denning, G.M., Anderson, M.P., Amara, J.F., Marshall, J., Smith, A.E. and Welsh, M.J., 1992. Processing of mutant cystic fibrosis transmembrane conductance regulator is temperature-sensitive. *nature*, 358(6389), pp.761-764.

Disterhoft JF, Thompson LT, Moyer JR Jr, Mogul DJ. 1996. Calcium-dependent afterhyperpolarization and learning in young and aging hippocampus. *Life Sci* 59:413–20

Dolphin AC. 2013. The alpha2delta subunits of voltage-gated calcium channels. *Biochim Biophys Acta – Biomembranes*, 1828 (7), 1541–1549.

Dolphin AC. A short history of voltage-gated calcium channels. *British journal of pharmacology*. 2006 Jan;147(Suppl 1):S56

Dolphin, A.C., 2018. Voltage-gated calcium channels: their discovery, function and importance as drug targets. *Brain and neuroscience advances*, 2, 2398212818794805

Fang K, Colecraft HM. 2011. Mechanism of auxiliary beta-subunit-mediated membrane targeting of L-type (Ca(V) 1. 2) channels. *J Physiol* 589:4437–4455.

Fatt, P. and Katz, B., 1953. The electrical properties of crustacean muscle fibres. *The Journal of physiology*, 120(1-2), p.171.

Feng, T., Kalyanamoorthy, S. and Barakat, K., 2018. L-type calcium channels: structure and functions. *Ion Channels in Health and Sickness*, 77305 p127-131. London: Intechopen. Shad, K.F. (Ed.).

Ferrari, A., Hoerndli, F., Baechli, T., Nitsch, R.M. and Götz, J., 2003.  $\beta$ -Amyloid induces paired helical filament-like tau filaments in tissue culture. *Journal of Biological Chemistry*, 278(41), pp.40162-40168.

Fichou, Y., Al-Hilaly, Y.K., Devred, F., Smet-Nocca, C., Tsvetkov, P.O., Verelst, J., Winderickx, J., Geukens, N., Vanmechelen, E., Perrotin, A. and Serpell, L., 2019. The elusive tau molecular structures: can we translate the recent

- breakthroughs into new targets for intervention?. *Acta neuropathologica communications*, 7(1), pp.1-17.
- Findeisen, F. and Minor Jr, D.L., 2009. Disruption of the IS6-AID linker affects voltage-gated calcium channel inactivation and facilitation. *Journal of General Physiology*, 133(3), pp.327-343.
- Foster TC. 1999. Involvement of hippocampal synaptic plasticity in age-related memory decline. *Brain Res Rev* 30:236–49.
- Foster, T.C. and Kumar, A., 2002. Calcium dysregulation in the aging brain. *The Neuroscientist*, 8(4), pp.297-301.
- Freshney, 2005. *Culture of Animal Cells (A Manual of Basic Technique)*. (Fifth edition).
- Geisler S, Schopf CL, Obermair GJ. 2014. Emerging evidence for specific neuronal functions of auxiliary calcium channel alpha2delta subunits.
- Gerstein, M., Lesk, A.M. and Chothia, C., 1994. Structural mechanisms for domain movements in proteins. *Biochemistry*, 33(22), pp.6739-6749.
- Goode, B.L., Denis, P.E., Panda, D., Radeke, M.J., Miller, H.P., Wilson, L. and Feinstein, S.C., 1997. Functional interactions between the proline-rich and repeat regions of tau enhance microtubule binding and assembly. *Molecular biology of the cell*, 8(2), pp.353-365.
- Hell, J.W., Westenbroek, R.E., Warner, C., Ahlijanian, M.K., Prystay, W., Gilbert, M.M., Snutch, T.P. and Catterall, W.A., 1993. Identification and differential subcellular localization of the neuronal class C and class D L-type calcium channel alpha 1 subunits. *The Journal of cell biology*, 123(4), pp.949-962.
- Hering, S., Berjukow, S., Sokolov, S., Marksteiner, R., Weiß, R.G., Kraus, R. and Hess P, Landsman J.B, Tsien R.W, 1984. Different modes of Ca channel gating behaviour favoured by dihydropyridine Ca agonists and antagonists. *Nature*. 1984;311:538–544
- Hess, P. and Tsien, R.W., 1984. Mechanism of ion permeation through calcium channels. *Nature*, 309(5967), pp.453-456.
- Hille, 1992. *Ionic channels of excitable membranes*, pg117.
- Hulme, J.T., Westenbroek, R.E., Scheuer, T. and Catterall, W.A., 2006. Phosphorylation of serine 1928 in the distal C-terminal domain of cardiac CaV1. 2 channels during  $\beta$ 1-adrenergic regulation. *Proceedings of the National Academy of Sciences*, 103(44), pp.16574-16579.
- Jadhav, S., Cubinkova, V., Zimova, I., Brezovakova, V., Madari, A., Cigankova, V. and Zilka, N., 2015. Tau-mediated synaptic damage in Alzheimer's disease. *Translational neuroscience*, 6(1), pp.214-226.

Jeganathan, S., von Bergen, M., Brutlach, H., Steinhoff, H. J., and Mandelkow, E. (2006). Global hairpin folding of tau in solution. *Biochemistry* 45, 2283–2293. doi: 10.1021/bi0521543

Johny, M.B., Yang, P.S., Bazzazi, H. and Yue, D.T., 2013. Dynamic switching of calmodulin interactions underlies Ca<sup>2+</sup> regulation of CaV1.3 channels. *Nature communications*, 4(1), pp.1-13.

Kametani, F. and Hasegawa, M., 2018. Reconsideration of amyloid hypothesis and tau hypothesis in Alzheimer's disease. *Frontiers in neuroscience*, 12, p.25.

Kass, R.S. and Arena, J.P., 1989. Influence of pH<sub>o</sub> on calcium channel block by amlodipine, a charged dihydropyridine compound. Implications for location of the dihydropyridine receptor. *The Journal of general physiology*, 93(6), pp.1109-1127.

Kay, B.K., Williamson, M.P. and Sudol, M., 2000. The importance of being proline: the interaction of proline-rich motifs in signaling proteins with their cognate domains. *The FASEB journal*, 14(2), pp.231-241.

Kimur, T., Hatsuta, H., Masuda-Suzukake, M., Hosokawa, M., Ishiguro, K., Akiyama, H., Murayama, S., Hasegawa, M., and Hisanaga, S.. (2016). The abundance of nonphosphorylated Tau in mouse and human tauopathy brains revealed by the use of phos- tag method. *American J. Pathology*. 186,398–409.

Koch, G. and Spampinato, D., 2022. Alzheimer disease and neuroplasticity. *Handbook of Clinical Neurology*, 184, pp.473-479.

Koch, G., Di Lorenzo, F., Bonni, S., Ponzio, V., Caltagirone, C. and Martorana, A., 2012. Impaired LTP-but not LTD-like cortical plasticity in Alzheimer's disease patients. *Journal of Alzheimer's Disease*, 31(3), pp.593-599.

Kwan, Y.W., Bangalore, R., Lakitsh, M., Glossmann, H. and Kass, R.S., 1995. Inhibition of cardiac L-type calcium channels by quaternary amlodipine: implications for pharmacokinetics and access to dihydropyridine binding site. *Journal of molecular and cellular cardiology*, 27(1), pp.253-262.

Lancaster, B., Adams, P.R., 1986. Calcium-dependent current generating the afterhyperpolarization of hippocampal neurons. *J. Neurophysiology*. 55, 1268–1282.

Larson, S.M. and Davidson, A.R., 2000. The identification of conserved interactions within the SH3 domain by alignment of sequences and structures. *Protein Science*, 9(11), pp.2170-2180.

Li, J., Li, Y., Liu, M. and Xie, S., 2020. Modified heptapeptide from tau binds both tubulin and microtubules. *Thoracic Cancer*, 11(10), pp.2993-2997.

Lima, P.A. and Marrion, N.V., 2007. Mechanisms underlying activation of the slow AHP in rat hippocampal neurons. *Brain research*, 1150, pp.74-82.

- Lipscombe, D., Helton, T.D. and Xu, W., 2004. L-type calcium channels: the low down. *Journal of neurophysiology*, 92(5), pp.2633-2641.
- Lopez, J.R., Lyckman, A., Oddo, S., LaFerla, F.M., Querfurth, H.W. and Shtifman, A., 2008. Increased intraneuronal resting  $[Ca^{2+}]$  in adult Alzheimer's disease mice. *Journal of neurochemistry*, 105(1), pp.262-271.
- Mahendran, T.S., Suresh, S.N., Garimella, L. and Manjithaya, R., 2020. Soluble 4R0N Tau Abrogates Endocytic Vesicular Dynamics. *Frontiers in Aging Neuroscience*, 12, p.537712.
- Marrion, N.V. and Tavalin, S.J., 1998. Selective activation of  $Ca^{2+}$ -activated  $K^{+}$  channels by co-localized  $Ca^{2+}$  channels in hippocampal neurons. *Nature*, 395(6705), pp.900-905.
- Matthews, E.A., Linardakis, J.M. and Disterhoft, J.F., 2009. The fast and slow afterhyperpolarizations are differentially modulated in hippocampal neurons by aging and learning. *Journal of Neuroscience*, 29(15), pp.4750-4755.
- Minati, L., Edginton, T., Grazia Bruzzone, M. and Giaccone, G., 2009. Reviews: current concepts in Alzheimer's disease: a multidisciplinary review. *American Journal of Alzheimer's Disease & Other Dementias®*, 24(2), pp.95-121.
- Morrison, K.L. and Weiss, G.A., 2001. Combinatorial alanine-scanning. *Current opinion in chemical biology*, 5(3), pp.302-307.
- Mroczo, B., Groblewska, M. and Litman-Zawadzka, A., 2019. The role of protein misfolding and tau oligomers (TauOs) in Alzheimer's disease (AD). *International Journal of Molecular Sciences*, 20(19), p.4661.
- Musacchio, A., 2002. How SH3 domains recognize proline. *Advances in protein chemistry*, 61, pp.211-268.
- Necula, M. and Kuret, J., 2004. Electron microscopy as a quantitative method for investigating tau fibrillization. *Analytical biochemistry*, 329(2), pp.238-246.
- Neely, A. and Hidalgo, P., 2014. Structure-function of proteins interacting with the  $\alpha 1$  pore-forming subunit of high-voltage-activated calcium channels. *Frontiers in physiology*, 5, p.209.
- Nimmrich, V. and Eckert, A., 2013. Calcium channel blockers and dementia. *British journal of pharmacology*, 169(6), pp.1203-1210.
- Norris, C.M., Korol, D.L. and Foster, T.C., 1996. Increased susceptibility to induction of long-term depression and long-term potentiation reversal during aging. *Journal of Neuroscience*, 16(17), pp.5382-5392.
- Núñez-Santana, F. L. et al. Surface L-type  $Ca^{2+}$  channel expression levels are increased in aged hippocampus. *Aging Cell* 13(1), 111–120 (2014).

Núñez-Santana, F.L., Oh, M.M., Antion, M.D., Lee, A., Hell, J.W. and Disterhoft, J.F., 2014. Surface L-type Ca<sup>2+</sup> channel expression levels are increased in aged hippocampus. *Aging Cell*, 13(1), pp.111-120.

Park, K., Begenisich, T. and Melvin, J.E., 2001. Protein kinase A activation phosphorylates the rat CIC-2 Cl<sup>-</sup> channel but does not change activity. *The Journal of membrane biology*, 182(1), pp.31-37.

Peterson, B.Z. and Catterall, W.A., 2006. Allosteric interactions required for high-affinity binding of dihydropyridine antagonists to Cav1.1 channels are modulated by calcium in the pore. *Molecular pharmacology*, 70(2), pp.667-675.

Picher, M.M., Opreșoreanu, A.M., Jung, S., Michel, K., Schoch, S. and Moser, T., 2017. Rab interacting molecules 2 and 3 directly interact with the pore-forming CaV1.3 Ca<sup>2+</sup> channel subunit and promote its membrane expression. *Frontiers in cellular neuroscience*, 11, p.160.

Portelius, E., Hansson, S.F., Tran, A.J., Zetterberg, H., Grognat, P., Vanmechelen, E., Höglund, K., Brinkmalm, G., Westman-Brinkmalm, A., Nordhoff, E. and Blennow, K., 2008. Characterization of tau in cerebrospinal fluid using mass spectrometry. *The Journal of Proteome Research*, 7(5), pp.2114-2120.

Pragnell M, De Waard M, Mori Y, Tanabe T, Snutch TP, Campbell KP. 1994. Calcium channel beta-subunit binds to a conserved motif in the I-II cytoplasmic linker of the alpha 1-subunit. *Nature* 368:67–70

Sahu, G. and Turner, R.W., 2021. The molecular basis for the calcium-dependent slow afterhyperpolarization in CA1 hippocampal pyramidal neurons. *Frontiers in Physiology*, 12. p.759707

Sallaberry, C.A., Voss, B.J., Majewski, J., Biernat, J., Mandelkow, E., Chi, E.Y. and Vander Zanden, C.M., 2021. Tau and membranes: Interactions that promote folding and condensation. *Frontiers in cell and developmental biology*, volume 9, p.2632.

Scheres, S.H., Zhang, W., Falcon, B. and Goedert, M., 2020. Cryo-EM structures of tau filaments. *Current Opinion in Structural Biology*, 64, pp.17-25.

Shafiei, S.S., Guerrero-Muñoz, M.J. and Castillo-Carranza, D.L., 2017. Tau oligomers: cytotoxicity, propagation, and mitochondrial damage. *Frontiers in aging neuroscience*, 9, p.83.

Shistik, E., Ivanina, T., Puri, T., Hosey, M. and Dascal, N., 1995. Ca<sup>2+</sup> current enhancement by alpha 2/delta and beta subunits in *Xenopus* oocytes: contribution of changes in channel gating and alpha 1 protein level. *The Journal of Physiology*, 489(1), pp.55-62.

Simms, B.A. and Zamponi, G.W., 2012. Trafficking and stability of voltage-gated calcium channels. *Cellular and Molecular Life Sciences*, 69(6), pp.843-856.

- Simms, B.A. and Zamponi, G.W., 2014. Neuronal voltage-gated calcium channels: structure, function, and dysfunction. *Neuron*, 82(1), pp.24-45.
- Skrabana, R., Sevcik, J., and Novak, M. (2006). Intrinsically disordered proteins in the neurodegenerative processes: formation of tau protein paired helical filaments and their analysis. *Cell. Mol. Neurobiol.* 26, 1085–1097. doi: 10.1007/s10571-006-9083-3
- Sotiropoulos, I., Galas, M.C., Silva, J.M., Skoulakis, E., Wegmann, S., Maina, M.B., Blum, D., Sayas, C.L., Mandelkow, E.M., Mandelkow, E. and Spillantini, M.G., 2017. Atypical, non-standard functions of the microtubule associated Tau protein. *Acta neuropathologica communications*, 5(1), pp.1-11.
- Stan, G.F., Church, T.W., Randall, E., Harvey, J.R.M., Brown, J.T., Wilkinson, K.A., Hanley G.J., Marrion, N.V., 2022. Tau isoform-specific enhancement of L-type calcium current and augmentation of afterhyperpolarisation in rat hippocampal neurones. *Nature Scientific Reports* 12:15231
- Stocker, M., Krause, M. and Pedarzani, P. 1999 An apamin-sensitive calcium activated potassium current in hippocampal pyramidal neurons. *Neurobiology*, 96 (8), 4662–4667
- Storm, J.F. 1987. Action potential repolarization and a fast after-hyperpolarization in rat hippocampal pyramidal cells. *J. Physiol.* 385:733-759.
- Striessnig, J. and Koschak, A., 2008. Exploring the function and pharmacotherapeutic potential of voltage-gated Ca<sup>2+</sup> channels with gene-knockout models. *Channels*, 2(4), pp.233-251.
- Striessnig, J., J Ortner, N. and Pinggera, A., 2015. Pharmacology of L-type calcium channels: novel drugs for old targets?. *Current molecular pharmacology*, 8(2), pp.110-122.
- Tang, L., Gamal El-Din, T.M., Payandeh, J., Martinez, G.Q., Heard, T.M., Scheuer, T., Zheng, N. and Catterall, W.A., 2014. Structural basis for Ca<sup>2+</sup> selectivity of a voltage-gated calcium channel. *Nature*, 505(7481), pp.56-61.
- Thomas, P. and Smart, T.G., 2005. HEK293 cell line: a vehicle for the expression of recombinant proteins. *Journal of pharmacological and toxicological methods*, 51(3), pp.187-200.
- Thompson, L.T., Deyo, R.A. and Disterhoft, J.F., 1990. Nimodipine enhances spontaneous activity of hippocampal pyramidal neurons in aging rabbits at a dose that facilitates associative learning. *Brain research*, 535(1), pp.119-130.
- Tikhonov, D.B. and Zhorov, B.S., 2009. Structural model for dihydropyridine binding to L-type calcium channels. *Journal of Biological Chemistry*, 284(28), pp.19006-19017

- Timin, E.N., 2000. Molecular determinants of inactivation in voltage-gated Ca<sup>2+</sup> channels. *The Journal of Physiology*, 528(2), pp.237-249.
- von Heijne, G., 1991. Proline kinks in transmembrane  $\alpha$ -helices. *Journal of molecular biology*, 218(3), pp.499-503.
- Wang, Z., Zhang, X. and Fedida, D., 2000. Regulation of transient Na<sup>+</sup> conductance by intra- and extracellular K<sup>+</sup> in the human delayed rectifier K<sup>+</sup> channel Kv1.5. *The Journal of physiology*, 523(3), pp.575-591.
- Woolfson, D.N. and Williams, D.H., 1990. The influence of proline residues on  $\alpha$ -helical structure. *FEBS letters*, 277(1-2), pp.185-188.
- Xu, W. and Lipscombe, D., 2001. Neuronal CaV1.3  $\alpha$ 1 L-type channels activate at relatively hyperpolarized membrane potentials and are incompletely inhibited by dihydropyridines. *Journal of Neuroscience*, 21(16), pp.5944-5951.
- Yang, L., Katchman, A., Morrow, J.P., Doshi, D. and Marx, S.O., 2011. Cardiac L-type calcium channel (Cav1.2) associates with  $\gamma$  subunits. *The FASEB Journal*, 25(3), pp.928-936.
- Yasojima, K., McGeer, E.G. and McGeer, P.L., 1999. Tangled areas of Alzheimer brain have upregulated levels of exon 10 containing tau mRNA. *Brain research*, 831(1-2), pp.301-305.
- Zamponi GW (2005). Voltage – gated calcium channels. Edn. Landes Bioscience/Eurekha.com;Kluwer Academic/Plenum Publishers: Georgetown, Tex. New York, N.Y.
- Zamponi, G.W., Striessnig, J., Koschak, A. and Dolphin, A.C., 2015. The physiology, pathology, and pharmacology of voltage-gated calcium channels and their future therapeutic potential. *Pharmacological reviews*, 67(4), pp.821-870.
- Zhang, H., Fu, Y., Altier, C., Platzer, J., Surmeier, D.J. and Bezprozvanny, I., 2006. CaV1.2 and CaV1.3 neuronal L-type calcium channels: differential targeting and signaling to pCREB. *European Journal of Neuroscience*, 23(9), pp.2297-2310.
- Zhang, J.F., Ellinor, P.T., Aldrich, R.W. and Tsien, R.W., 1994. Molecular determinants of voltage-dependent inactivation in calcium channels. *Nature*, 372(6501), pp.97-100
- Zhong, Q., Congdon, E.E., Nagaraja, H.N. and Kuret, J., 2012. Tau isoform composition influences rate and extent of filament formation. *Journal of Biological Chemistry*, 287(24), pp.20711-20719.